[American Journal of Science, Vol. 318, September, 2018, P. 764–798, DOI 10.2475/07.2018.02]

THE TECTONICS AND PALEO-DRAINAGE OF THE EASTERNMOST HIMALAYA (ARUNACHAL PRADESH, INDIA) RECORDED IN THE SIWALIK ROCKS OF THE FORELAND BASIN

GWLADYS GOVIN*, YANI NAJMAN*,†, GUILLAUME DUPONT-NIVET**,***,§, IAN MILLAR§§, PETER VAN DER BEEK§§§, PASCALE HUYGHE§§§, PAUL O'SULLIVAN‡, CHRIS MARK‡‡, and NATALIE VÖGELI§§§

ABSTRACT. The Siwalik sedimentary rocks of the Himalayan foreland basin preserve a record of Himalayan orogenesis, paleo-drainage evolution, and erosion. This study focuses on the still poorly studied easternmost Himalaya Siwalik record located directly downstream of the Namche Barwa syntaxis. We use luminescence, palaeomagnetism, magnetostratigraphy, and apatite fission-track dating to constrain the depositional ages of three Siwalik sequences: the Sibo outcrop (Upper Siwalik sediments at *ca.* 200–800 ka), the Remi section (Middle and Upper Siwalik rocks at >0.8–<8.8±2.4 Ma), and the Siang section (Middle Siwalik rocks at <9.3±1.5 to <13.5±1.5 Ma). Cretaceous-Paleogene detrital zircon and apatite U-Pb ages, characteristic of the Transhimalayan Gangdese Batholiths that crop out northwest of the syntaxis, are present throughout the Sibo, Remi, and Siang successions, confirming the existence of a Yarlung-Brahmaputra connection since at least the Late Miocene. A *ca.* 500 Ma zircon population increases up section, most strikingly sometime between 3.6 to 6.6 Ma, at the expense of Transhimalayan grains. We consider the *ca.* 500 Ma population to be derived from the Tethyan or Greater Himalaya, and we interpret the up-section increase to reflect progressive exhumation of the Namche Barwa syntaxis. Early Cretaceous zircon and apatite U-Pb ages are rare in the Sibo, Remi, and Siang successions, but abundant in modern Siang River sediments. Zircons of this age range are characteristic of the Transhimalayan Bomi-Chayu batholiths, which crop out east of the syntaxis and are eroded by the Parlung River, a modern tributary of the Siang River. We interpret the difference in relative abundance of Early Cretaceous zircons between the modern and ancient sediments to reflect capture of the Parlung by the Siang after 800 ka.

Key words: Himalaya, Siwaliks, Namche Barwa syntaxis, Brahmaputra River, Parlung River, detrital geochronology and thermochronology.

INTRODUCTION

The study of Himalayan foreland basin sedimentary rocks provides important complementary information to bedrock analysis for the understanding of orogenesis. It is particularly valuable where bedrock regions are inaccessible, or where the early record of metamorphism and exhumation has been lost in the bedrock record due to overprinting by later metamorphism or removal by erosion. In the Himalaya, Neogene-Quaternary sedimentary rocks of the Siwalik Group form an apron along the southern flank of the range (for example, Burbank and others, 1996). The sedimentary record of material eroded from the orogen and preserved in the Siwalik Group documents evidence of the tectonic (for example, DeCelles and others, 1998; Szulc and others,

* Lancaster Environment Centre, Lancaster University, United Kingdom
** Géosciences Rennes UMR-6118, CNRS - Université de Rennes 1, France
*** Department of Earth and Environmental Sciences, Potsdam University, Germany
§ Key Laboratory of Orogenic Belts and Crustal Evolution, Ministry of Education, Beijing, China
§§ Geochronology and Tracers Facility, NIGL, British Geological Survey, Keyworth, United Kingdom
§§§ ISTerre, Université Grenoble Alpes, Grenoble, France
‡ GeoSep Services, Moscow, Idaho 83843, USA
‡‡ Irish Centre for Research in Applied Geosciences (iCRAG), Department of Geology, Trinity College Dublin, Dublin, Ireland
† Corresponding author: y.najman@lancaster.ac.uk

2006; Coutand and others, 2016; Lang and others, 2016), erosional (for example, Harrison and others, 1993; Bernet and others, 2006; van der Beek and others, 2006; Chirouze and others, 2013) and climatic (for example, Quade and others, 1995; Vögeli and others, 2017a) evolution of the hinterland. However, relatively little work has been carried out in the easternmost Himalaya, either on bedrock (notable exceptions being the publications of Verma, 1999 and papers therein; Yin and others, 2006, 2010; Webb and others, 2013; DeCelles and others, 2016) or in the foreland basin (see work by Cina and others, 2009; Chirouze and others, 2013; Lang and Huntington, 2014; Lang and others, 2016; Vögeli and others, 2017b). Yet this is an important region, different from the main arc of the orogen because of: (1) its termination against the anomalously young and rapidly exhuming Namche Barwa syntaxial massif to the east (for example, Zeitler and others, 2014); (2) the potential influence on the basin of the westward encroaching Indo-Burman Ranges (IBR; Maurin and Rangin, 2009); and (3) the debated extent to which the geology of the eastern Himalayas replicates that along-strike to the west (Yin and others, 2006; DeCelles and others, 2016).

The present study aims to go some way towards rectifying this lack of information through investigation of the most easterly foreland-basin sedimentary rocks yet studied, located directly downstream of, and most proximal to, the eastern Himalayan syntaxis. We constrain the depositional age frame of the sedimentary record using magnetostratigraphy, detrital apatite fission-track (AFT) dating, infrared-stimulated luminescence (IRSL) and palaeomagnetism. We assess the provenance of these deposits using U-Pb dating of apatite and zircon, dating both grain cores and rim overgrowths for the latter.

BACKGROUND

Main Geologic Features of the Himalaya

The collision between the Indian and Asian plates in Late Paleocene to Early Eocene times (Najman and others, 2010; DeCelles and others, 2014; Hu and others, 2015) and the associated crustal thickening and shortening has led to the formation of the Himalayan belt (Le Fort, 1975; Hodges, 2000; Yin and Harrison, 2000) (fig. 1). Collision took place along the Indus-Yarlung suture zone (IYSZ), which juxtaposes the remnants of the pre-collision Indian passive margin sequence to the south and the Transhimalayan Asian batholiths of the Lhasa Block and Neo-Tethyan ophiolites to the north (Hébert and others, 2012 and references therein). The Mesozoic-Paleogene Transhimalayan Andean-type batholiths adjacent to the Indus-Yarlung suture zone (Chu and others, 2006) provide evidence for an Andean-style margin prior to collision. The Transhimalayan rocks in the eastern Himalaya include the Cretaceous-Paleogene Gangdese and Bomi-Chayu batholiths (for example, Chiu and others, 2009; Wang and others, 2014).

South of the Indus-Yarlung suture zone, north-dipping crustal faults extending throughout the entire E-W Himalayan arc separate the main Himalayan units (for example, Le Fort, 1975; Hodges, 2000; Yin and Harrison, 2000). The Tethyan Himalayan Sequence is composed of Paleozoic to Eocene sedimentary to low-grade metasedimentary rocks deposited on the northern Indian pre-collision passive margin. The medium- to high-grade metamorphic rocks (schists, gneisses, and migmatites) of the Greater Himalayan Sequence (GHS) crop out south of the Tethyan Himalayan Sequence and are separated from it by the extensional South Tibetan Detachment (STD). Both the Greater Himalayan Sequence and Tethyan Himalaya are intruded by Miocene leucogranites. The GHS is bounded by the Main Central Thrust (MCT) to the south. Post-collisional metamorphism and subsequent exhumation of the GHS along the MCT predominantly took place in the Early-Mid Miocene (Godin and others, 2006; Kellett and others, 2013), with local reactivation of the MCT in the Late Miocene

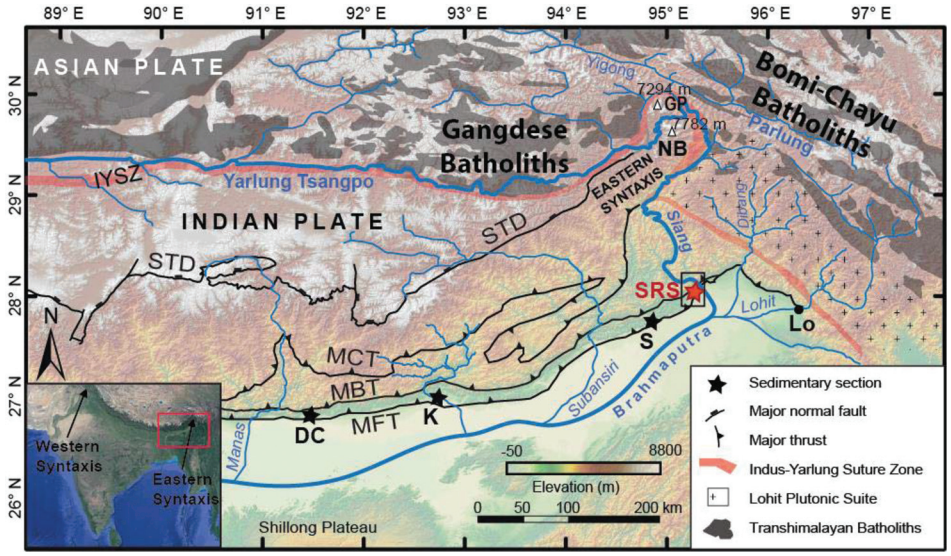

Fig. 1. Digital elevation model and main geologic features of the eastern Himalaya (modified from Lang and Huntington, 2014; Govin and others, 2018 and references therein). The red star labeled SRS represents the locations of the Sibo, Remi and Siang sections; the black stars show other dated Siwalik sections in the eastern Himalaya: S - Siji, K - Kameng and DC - Dungsam Chu. Lo indicates the Lohit modern river sample from Cina and others (2009). Black box indicates location of figure 2. Abbreviations are: NB - Namche Barwa, GP - Gyala Peri, MFT - Main Frontal Thrust, MCT - Main Central Thrust, MBT - Main Boundary Thrust, STD - South Tibetan Detachment and IYSZ - Indus-Yarlung Suture Zone.

(Catlos and others, 2004; Anczkiewicz and others, 2014; Braden and others, 2017, 2018).

South of the MCT, the Lesser Himalayan Sequence (LHS) is composed of predominantly low-grade Proterozoic meta-sedimentary rocks along with upper-Paleozoic, Mesozoic and Paleogene sedimentary rocks. Both the Greater and Lesser Himalayan Sequences are part of the Indian plate. Initiation of exhumation of the Lesser Himalayan duplex commenced around 10 to 12 Ma (for example, DeCelles and others, 2016 and references therein).

South of the LHS, the Sub-Himalayan sedimentary fold-and-thrust belt is bounded by the Main Boundary Thrust (MBT) to the north and the Main Frontal Thrust (MFT) to the south. The Sub-Himalaya consists of the Neogene to Quaternary clastic sedimentary rocks of the Siwalik Group. Undeformed Recent deposits of the Himalayan foreland basin occur south of the Main Frontal Thrust (Gansser, 1983; Hodges, 2000).

Structure of the Eastern Himalaya

The main arc of the orogen.—The extent to which the geology described above is representative of the far eastern Himalaya is debated (Yin and others, 2006; DeCelles and others, 2016). At a broad scale, the geology is similar: the main units of the Transhimalaya, Greater, Lesser and Sub-Himalaya are represented, divided by the same major thrusts as documented further west. In detail, DeCelles and others (2016) divided the region south of the Tethyan Himalaya into the Subhimalayan imbricate zone, Lesser Himalayan imbricate zone, Bomdila imbricate zone and Greater Himalayan zone. The Siwalik rocks of the Subhimalaya are described in the section *Sedimentary Record of the Eastern Himalaya* below. The Lesser Himalaya is bounded to the south by the MBT and to the north by the Bome Thrust. The rocks of this unit are comprised of

Paleoproterozoic Lower Lesser Himalayan siliclastics of the Daling and Shumar Formations, intruded by the Bomdila orthogneiss, Neoproterozoic-Paleozoic Upper Lesser Himalayan meta-sediments of the Baxa Group and Diuri Formation, and Permian siliciclastic rocks of the Gondwana Group (for example, McQuarrie and others, 2008; Long and others, 2012; DeCelles and others, 2016). Structurally overlying the Gondwana Group, the Bomdila imbricate zone consists of Lower Lesser Himalayan rocks and Phanerozoic rocks of the Rupa Group, proposed to be equivalent to Tethyan strata (DeCelles and others, 2016). Further north lie the rocks of the GHS, separated from the units below by the MCT. The timing of movement along the various thrusts (as summarized by DeCelles and others, 2016) is not well known, partly relies on extrapolation of data from Bhutan, and broadly follows the timings outlined in the section above for the main arc of the orogen.

The Namche Barwa and eastern syntaxis.—At the eastern termination of the Himalaya, the structural trend bends around the eastern syntaxis, changing from E-W to N-S striking (fig. 1). According to the map of Zeitler and others (2014), the Tethyan and Greater Himalaya terminate against the syntaxis, and do not crop out east of it.

In the core of the syntaxis, the Namche Barwa and the Gyala Peri massifs reach elevations of >7 km (fig. 1). This region is dominated by extreme relief and deep, steep gorges. The Tsangpo gorge, a <200-m wide, 200-km long fluvial knick-zone descending >2 km between the Namche Barwa and the Gyala Peri peaks, is one of the deepest on Earth (for example, Zeitler and others, 2001; Larsen and Montgomery, 2012; Lang and others, 2013). The Namche Barwa massif is the locus of young (<10 Ma) high-grade metamorphism, melting and extreme rates of exhumation of up to 5 to 10 km/Myr (Booth and others, 2004, 2009; Seward and Burg, 2008; Zeitler and others, 2014). In comparison, peak metamorphism in the main arc of the range occurred in the Early Miocene, and lower exhumation rates of ≤~2 km/Myr are typical (for example, Thiede and Ehlers, 2013 and references therein). Bedrock thermochronology data from the Namche Barwa massif have been interpreted to indicate that very rapid exhumation started at 3 to 4 Ma (Seward and Burg, 2008) or 8 to 10 Ma (Zeitler and others, 2014). Detrital studies have inferred ages of ~7 Ma to <3 Ma (Chirouze and others, 2013; Bracciali and others, 2016; Lang and others, 2016) for the onset of rapid exhumation in the Namche Barwa massif. The massif constitutes an antiformal structure, exposing high-grade metamorphic rocks of Tethyan / GHS origin (Burg and others, 1997). The north-plunging antiform characterizing the Namche Barwa massif has been suggested to have expanded both vertically and laterally through time, and to have migrated northward since its initiation (Seward and Burg, 2008; Bracciali and others, 2016; King and others, 2016).

The Indo-Burman Ranges.—East of the syntaxis, structures trend northwest-southeast in the northern Indo-Burman Ranges (IBR; Haproff and others, 2018; fig. 1). The IBR are considered to constitute an accretionary prism formed as the Indian plate is being subducted obliquely beneath Asia (Curray and others, 1979). They consist of a belt of predominantly Paleogene rocks to the east, and a Neogene belt to the west. The Paleogene rocks consist of turbidites predominantly derived from the Burmese arc to the east, which can be considered as a continuation of the southern margin of Asia north of the Yarlung suture zone. The Neogene rocks are considered to be recycled Himalayan-derived Bengal Fan material (Allen and others, 2008). The timing of exhumation of the eastern IBR is poorly constrained to Paleogene times (Licht and others, 2013, 2016). Westward propagation of the thrust belt ensued, with recent thrusting dated at ~2 Ma at the ranges' most westward extent (Maurin and Rangin, 2009; Najman and others, 2012).

Drainage of the Eastern Himalaya

The Brahmaputra River is sourced at Mount Kailash in southern Tibet and flows more than 1000 km eastwards along the suture zone as the Yarlung Tsangpo. It crosses the range to the south and turns 180° after incising a deep gorge between the Gyala Peri and the Namche Barwa massifs. At this bend the river connects with the tributary Parlung River to the north, which is itself connected to the Yigong River a few tens of kilometers upstream (fig. 1). The Yigong River flows toward the southeast whereas the Parlung River upstream of its confluence with the Yigong River flows toward the NW and drains the Bomi-Chayu batholiths ENE of the eastern syntaxis (fig. 1). Downstream of the Namche Barwa massif, the Yarlung Tsangpo becomes the Siang River until it reaches the foreland basin in Arunachal Pradesh, where it becomes the Brahmaputra River. In the foreland, the tributary Lohit River, flowing SW and also draining the Bomi-Chayu batholith in its upland catchment, connects with the Brahmaputra River along with other eastern tributaries, which drain the Lohit plutonic suite and IBR, and western tributaries, some of which drain as far north as the Tethyan Himalaya (fig. 1).

The evolution of the complex drainage pattern in the eastern Himalayan region remains incompletely understood. This river network is suggested to result from drainage reorganization as a consequence of river-capture and -reversal events (Clark and others, 2004; Clift and others, 2006). The Brahmaputra River captured the Yarlung Tsangpo in Early Miocene times (Lang and Huntington, 2014; Bracciali and others, 2015) and has been feeding the Bengal Fan since at least this time (Blum and others, 2018). It has been proposed that, prior to capture, the paleo-Yarlung-Tsangpo flowed further to the east into the Red and/or Irrawaddy rivers, potentially via the Parlung River, and was sequentially rerouted by various capture events down the Lohit, Dibang and Siang rivers (Brookfield, 1998; Clark and others, 2004; Robinson and others, 2014). This scenario has been questioned, however (for example, Licht and others, 2013; Wang and others, 2014) and internal drainage of the Yarlung Suture zone basin has also been proposed for the Paleogene (for example, Leary and others, 2016). The drainage evolution since Miocene times involves various hypotheses, such as the Yarlung flowing through the Parlung River to the Irrawaddy River prior to its capture by the Siang through headward erosion, leading to Parlung River reversal (Clark and others, 2004). Alternatively, recent studies have argued that the Parlung-Yarlung connection postdates the establishment of the Yarlung-Siang connection and occurred during the Quaternary (Lang and Huntington, 2014; King and others, 2016), possibly related to lateral propagation of the Namche Barwa massif (Seward and Burg, 2008). Lang and Huntington (2014) proposed that prior to this capture event, a paleo-Parlung-Lohit connection existed upstream of the Brahmaputra-Lohit confluence.

Source Characterizations of the Eastern Himalaya

The Yarlung River and tributaries drain the Transhimalayan Gangdese and Bomi-Chayu batholiths of the Asian Lhasa block. The Transhimlaayan Gangdese rocks have distinct compositional and age characteristics (as recorded by whole-rock Sr and Nd isotope ratios as well as Hf isotopic signatures and U-Pb ages of zircons, for example Ji and others, 2009), different from rocks of the Indian plate Himalayan units south of the Indus-Yarlung Suture Zone.

The Himalayan units are largely composed of Proterozoic-Eocene rocks that were variably metamorphosed during the Cenozoic, and intruded by late Oligocene to Miocene leucogranites (DeCelles and others, 2004; Gehrels and others, 2011). All rocks of the Indian plate, that is Tethyan, Greater and Lesser Himalaya, are typified by a majority of zircons of Early Paleozoic and Precambrian age. The units differ in the

paucity of 500-Ma grains in the Lesser Himalaya, which has an abundance of grains >1800 Ma (for example, Gehrels and others, 2011).

These ages from the Indian plate are shared by the Asian plate Lhasa Block substrate (for example, Zhang and others, 2012 and references therein) but contrast with the typically Cretaceous-Early Paleogene zircons of the Transhimalayan batholiths that comprise the majority of the southern Asian margin in this region (for example, Chu and others, 2006; Mo and others, 2007; Robinson and others, 2014 and references therein). Regional differences exist: a Paleogene (~50 Ma) peak is prominent whilst Early Cretaceous ages are poorly represented in the southern Transhimalayan Gangdese batholith, which contributes to the zircon U-Pb signal of the modern Yarlung River (Zhang and others, 2012; Carrapa and others, 2017). By contrast, Early Cretaceous zircons are prominent in the continuation of this previously active margin to the east: they are abundant in the Bomi-Chayu igneous sources east of the Namche Barwa syntaxis (Booth and others, 2004; Liang and others, 2008; Chiu and others, 2009; Xu and others, 2012; Zhang and others, 2012; Haproff and others, 2013; Lang and Huntington, 2014). The Lohit Plutonic Suite (fig. 1) has been suggested to be a source of Early- and Late-Cretaceous zircons (Cina and others, 2009; Haproff and others, 2013), as evidenced by the zircon U-Pb ages in the Lohit River (Cina and others, 2009; Zhang and others, 2012) and a prominent population of this age is also recorded in the Dhansiri River draining the northern IBR (Bracciali and others, 2015).

This characterization of zircon U-Pb ages has allowed partial reconstruction of the paleo-drainage system in the eastern Himalayan region (for example, Cina and others, 2009; Lang and Huntington, 2014; Bracciali and others, 2015). Whilst zircon U-Pb dating is widely used in the eastern Himalaya, little apatite U-Pb dating has yet been performed in the Himalaya. Therefore, apatite U-Pb age characterization of both the eastern syntaxis and the Transhimalayan batholith source remains relatively unconstrained. To our knowledge, existing Himalayan apatite U-Pb data is limited to: (1) bedrock samples from the Lesser and Greater Himalaya in the upper Indus catchment (Turab and others, 2017): Greater Himalayan apatite yields ages from *ca.* 17 to 42 Ma; Lesser Himalayan apatites yield predominantly Proterozoic ages. (2) Modern river sediment (MRS) samples collected from the Marsyandi and Siang rivers (Najman and others, in review[1]): the Siang yields a main modal age peak at *ca.* 25 Ma, and smaller peaks at *ca.* 13 and 6 Ma; the Marsyandi yields modal peaks at *ca.* 22 and 61 Ma, with a small number of Proterozoic ages. The youngest ages from the Marsyandi are *ca.* 12 Ma; we therefore consider the *ca.* 6 Ma Siang peak as potentially diagnostic of the syntaxis. (3) Detrital samples from Miocene – Quaternary units sampled from the Bengal fan by IODP354 (Najman and others, in review), which cannot readily be used for source area characterization.

The Namche Barwa massif of the eastern syntaxis is characterized by very young (10 to <1 Ma) mineral-growth and -cooling ages (Burg and others, 1998; Ding and others, 2001; Booth and others, 2004, 2009; Finnegan and others, 2008; Zeitler and others, 2014; Bracciali and others, 2016). These diagnostic ages, and their consequent short lag times in the foreland basin sedimentary rocks, have been used in the eastern Himalayan foreland basin to track eastern syntaxis detritus (Bracciali and others, 2016; Lang and others, 2016).

Sedimentary Record of the Eastern Himalaya

The Siwalik Group in the Himalayan foreland is divided into three informal units based on sedimentary facies: the Lower, Middle and Upper Siwalik rocks (Burbank and

[1] Najman, Y., Mark, C., Barfod, D., Carter, A., Parrish, R., Chew, D., and Gemignani, L., Spatial and temporal trends in exhumation of the Eastern Himalaya and syntaxis as determined from a multi-technique detrital thermochronological study of the Bengal Fan: Geological Society of America Bulletin, in review.

others, 1996; DeCelles and others, 1998). These informal units locally correspond to formally defined formations, that is, respectively the Dafla, Subansiri and Kimin Formations in Arunachal Pradesh (Chirouze and others, 2012; DeCelles and others, 2016 and references therein). Up-section coarsening in the Siwalik rocks of the eastern Himalaya is interpreted as recording the progressive transition from deposition by low-gradient sinuous channels in a fluvio-deltaic setting to deposition by steep braided rivers in alluvial fans along the Himalayan front, as the thrust front propagated southward. The Lower Siwalik rocks are mainly composed of alternating fine-grained sandstones and siltstones with common leaf-impressions and paleosols, interpreted in this area as deposited in a fluvio-deltaic plain environment. The Middle Siwalik rocks, interpreted as a braided fluvial facies, consist of massive medium- to coarse-grained sandstone layers, with frequent cross-bedding, soft-sedimentary deformation and increasing occurrence of conglomerates up-section. The Upper Siwalik rocks are mainly composed of conglomerates interbedded with sandstones and some siltstones, interpreted as pebbly braided-river deposits (for example, Cina and others, 2009; Chirouze and others, 2012; Lang and Huntington, 2014; Coutand and others, 2016).

Only three Siwalik sections have hitherto been dated by magnetostratigraphy in the eastern foreland basin (fig. 1): the Dungsam Chu section in Bhutan (Coutand and others, 2016), the Kameng section in western Arunachal Pradesh (Chirouze and others, 2012), and the Siji section (Likabali) in eastern Arunachal Pradesh (Lang and others, 2016). In these sections, the oldest Lower Siwalik sedimentary rocks have been dated at *ca.* 13 Ma, with a Lower-Middle Siwalik transition estimated at *ca.* 10.5 Ma in the Kameng (Chirouze and others, 2012), whilst the same transition is dated at 6 Ma in the Dungsam Chu section (Coutand and others, 2016). Lower Siwalik rocks are not reported in the 4600-m-thick Siji composed of Middle and Upper Siwalik rocks only (Lang and others, 2016). The Middle-Upper Siwalik transition (where the base of the Upper Siwalik rocks is defined as the first occurrence of massive conglomerate layers) varies from ~3.8 Ma in the Dungsam Chu section (Coutand and others, 2016), 2.5 Ma in the Kameng section (Chirouze and others, 2012) and <2 Ma in the Siji section (Lang and others, 2016).

THE SIBO, REMI, AND SIANG SUCCESSIONS

We have studied Siwalik sedimentary rocks at three different locations (Remi, Sibo and Siang) within a 20 km-long segment along the eastern Himalayan front (fig. 2). Middle and Upper Siwalik rocks are exposed at these locations, as defined by lithostratigraphic correlation with other sections throughout the basin as described above. These are the most easterly dated sections of the Siwalik Group, with the Siang section located where the modern Siang River reaches the foreland basin. The main sedimentary characteristics in these locations are similar to the Upper and Middle Siwalik sedimentary rocks of the eastern Himalaya described previously; more detailed sedimentological descriptions are presented in table 1.

Sibo Outcrop

The Sibo outcrop exposes *ca.* 20 stratigraphic meters of Upper Siwalik sediments tilted 10° towards the NW. A large-scale channel fill is clearly observed in the upper part of the outcrop. In the lowermost part of the outcrop, the sands contain a significant amount of muscovite; in contrast, no muscovite has been observed in the sandy matrix of the nearby conglomerates. The dominant conglomerate clast material in the Sibo section is quartz-arenite with a minor amount of other sandstone and volcanic clasts. The modern Sibo riverbed comprises numerous quartz-arenite pebbles with subordinate basalt and other sandstone clasts.

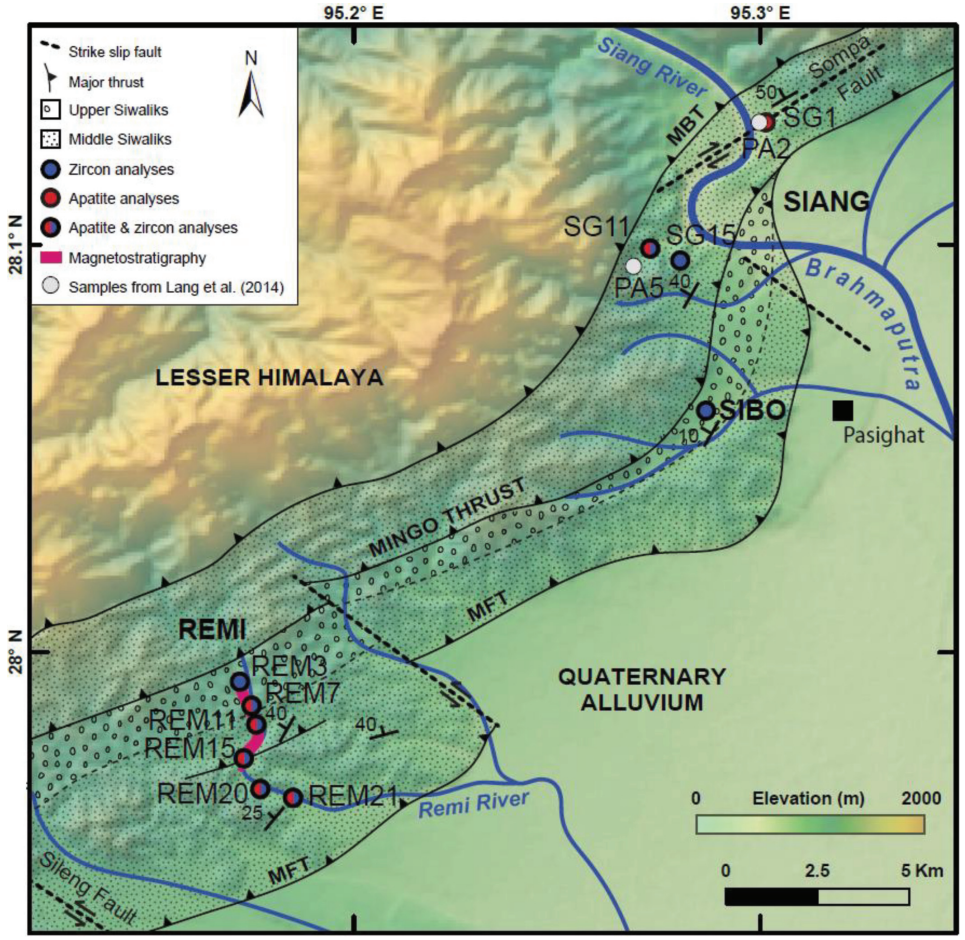

Fig. 2. Digital elevation model and main geologic features of the study area (modified after Luirei and Bhakuni, 2008 and Srivastava and others, 2009). Samples are indicated according to the method applied (mineral analyzed); samples in white are from Lang and Huntington (2014), samples in blue and red are from this study.

Remi Section

The Remi section is composed of *ca.* 700 m of Upper Siwalik rocks and 1200 m of Middle Siwalik rocks, homoclinally tilted ~40° towards the NW (fig. 3). The section is bounded to the north by the north-dipping Mingo Thrust and to the south by the Main Frontal Thrust (fig. 2). A minor north-dipping thrust in the upper part of the Middle Siwalik succession has also been observed (below and south of sample REM15 in figs. 2 and 3, respectively). The Siwalik rocks in the Remi section coarsen upsection, from medium-grained sandstones to conglomerates. The sandstones are often weathered and poorly indurated. Apart from cross-bedding, features indicating paleocurrent directions are rare. It was not possible to precisely measure paleo-current directions in the section. Wood fragments, bioturbation, current-generated features and laminations are recorded in the lower part of the section, below the conglomerates; root traces and current-generated features are uncommonly recorded in the sandstones interbedded with the conglomerates

TABLE 1

Sedimentological descriptions of Siwalik sedimentary rocks from the Sibo, Remi and Siang locations, eastern Arunachal Pradesh

LOCATION	UNIT	LITHOLOGY	SEDIMENTARY FEATURES	CLASTS
SIBO	Upper Siwaliks	Medium to coarse-grained sandstones, coarsening up-section, alternating with conglomerates, the proportion of which increases up-section	Very few lenses of clays	Sub-angular to well rounded; 10-170 mm long axis; 5-90 mm short axis
REMI	Upper Siwaliks	Interlayered medium-grained sandstones and conglomerates. Thickness of conglomerate bands increases up-section to reach several meters; matrix grain size also coarsens up-section	Occasional finer-grained layers from claystones to fine-grained sandstones; frequent coal fragments	Sub-angular to rounded; 5- 95 mm short axis; 10-130 mm long axis
	Middle Siwaliks	Cliffs up to 20 m high of "salt and pepper" medium-grained to pebbly sandstones. Sandstone beds are up to tens of meters thick. Coarsening up- section with an increasing occurrence of pebbly material	Occasional pebbly layers at the base of sandstone beds; intercalated silt or mud lenses. Common large-scale cross- bedding, fossil wood and coal fragments; medium-grained sandstones occasionally bioturbated	Angular to rounded; 5-65 mm short axis; 5-100 mm long axis
SIANG	Middle Siwaliks **East bank**	Cliffs up to 20 m high of medium to coarse-grained "salt and pepper" and orange-weathered colored sandstone. Mica rich sandstones overlain by Quaternary conglomeratic terraces. Occurrence of pebbles, the proportion of which increases up-section	Common carbonized fossil wood of millimeter- to meter size (up to 3.80 m); frequent cross bedding and centimeter- scale diagenetic nodules; occasional roots and bioturbation, ripple marks and channels; common wood fragments	Centimeter-scale siltstone pebbles (2-30 cm long axis); millimeter- to centimeter- scale quartz- arenite pebbles at the base of the sand beds; presence of a meter thick quarzitic conglomerate bed (clast sizes of 5-10 cm).
	Middle Siwaliks **West bank**	Greenish to light gray salt and pepper fine to coarse-grained sandstone; containing muscovite, biotite, garnet, amphiboles, hornblende	Less indurated, compared with the east bank, indistinct bedding, finer-grained and more weathered	Presence of coal

in the upper part of the section. The conglomerate clasts from the Remi section are predominantly composed of quartz-arenite, and subordinately other sandstones, siltstones and volcanics, whereas the modern Remi riverbed material is mainly composed of gneiss and quartz-arenite pebbles.

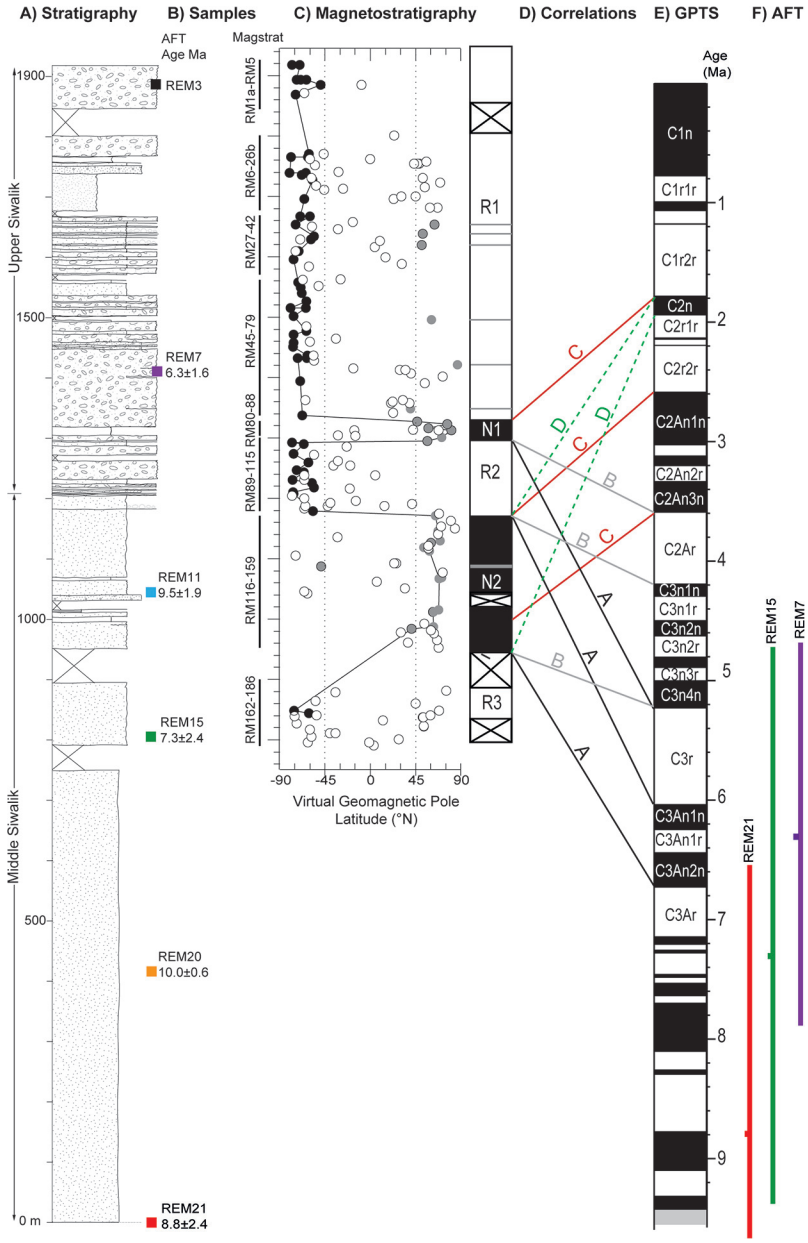

Fig. 3. Remi section showing magnetostratigraphic results and age models. (A) Lithostratigraphic column. (B) Stratigraphic position of samples for Apatite Fission Track (AFT) dating with Maximum Depositional Age and for magnetostratigraphy (Magstrat). (C) Magnetostratigraphic results. Black dots for reliable Q1 and Q2 ChRM of reversed polarity direction. Gray dots with black outlines are Q1 normal polarity directions and isolated Q2 reversed polarity directions. Plain gray dots indicate Q2 normal polarity directions. Open circles depict unreliable Q3 and Q4 directions. The polarity column is defined from our magnetostratigraphic measurements; black and white intervals indicate normal (N) and reverse (R) polarity zones, respectively. Gray intervals represent poorly constrained polarities defined by only one sample. Intervals with a cross indicate gaps in the sampling or in polarity determination. (D) Proposed correlations of the polarity column to the geomagnetic polarity time scale (GPTS) of Gradstein and others (2012). (E) GPTS created using TSCreator v.6.4 software from https://engineering.purdue.edu/Stratigraphy/tscreator/index/index.php, based on time scale of Gradstein and others (2012). (F) Maximum Depositional Ages determined with Apatite Fission Tracks (AFT) for the samples shown in (B) relevant to constrain the correlations.

Siang Section

The Siang section is crossed by the Siang River, and is therefore composed of two separate outcrops located on the east and west banks of the river (fig. 2). On both banks, medium- to coarse-grained sandstones typical of Middle Siwalik rocks crop out, dipping 35 to 55° to the NW, in tectonic contact with the Lesser Himalayan Series to the north along the Main Boundary Thrust. The west-bank outcrop appears more weathered and finer-grained than the east-bank outcrop. Additionally, the bedding orientation with respect to the location of both outcrops leads us to suggest an older age for the west-bank outcrop in comparison with the east-bank outcrop. Pebble beds, wood fragments, current-generated features, ripple marks and bioturbation are recorded. The modern Siang riverbed is mainly composed of pebbles and boulders of quartz-arenite, mafic volcanics, metasedimentary, carbonate and plutonic rocks, with subordinate gneisses, meta-breccias and other sandstones.

METHODS

Stratigraphic Dating

In order to date the deposition of the sedimentary rocks from the Sibo, Remi, and Siang successions, we used palaeomagnetic and luminescence dating for the Sibo outcrop, apatite fission-track dating to determine maximum depositional ages for the Remi and Siang sections, and magnetostratigraphy to date the upper part of the Remi section. Detailed methodology is given in Supplementary Materials 1 (http://earth.geology.yale.edu/%7eajs/SupplementaryData/2018/Govin), and sample locations are given in Supplementary Materials 2 (http://earth.geology.yale.edu/%7eajs/SupplementaryData/2018/Govin).

Paleomagnetic and luminescence dating.—Two core samples from the Upper Siwalik sediments at Sibo were analyzed to determine their magnetic polarity, using the paleomagnetic method described below and in Supplementary Materials 1. Another drill-core sample was prepared for luminescence dating at the University of Bern (Switzerland) to refine the age of these sediments. This sample was prepared and analyzed along with samples from Abrahami and others (2018), with the same methodology and in the same conditions (see Supplementary Materials 1 for details). Additional data are presented in Supplementary Materials 3 (http://earth.geology.yale.edu/%7eajs/SupplementaryData/2018/Govin).

Apatite fission-track dating.—Apatite fission-track (AFT) analysis was carried out to constrain the maximum depositional ages for sedimentary rocks from the Remi and Siang sections. Six medium- to coarse-grained sandstones from the Remi section and two from the Siang section were sampled at regular stratigraphic intervals (fig. 3). The youngest sample from the Remi section (REM3) did not contain sufficient apatite to allow robust dating. Apatite separation was performed at ISTerre, Université Grenoble Alpes (France) using standard techniques; fission-track analysis (and simultaneous U-Pb analysis, see below) was performed by GeoSep Services (USA) using the laser-ablation-inductively coupled plasma-mass spectrometry (LA–ICP–MS) method (Donelick and others, 2005). Full details of sample preparation and analytical procedures are provided in Supplementary Materials 1 together with data tables in Supplementary Materials 4 (http://earth.geology.yale.edu/%7eajs/SupplementaryData/2018/Govin).

The youngest age peak for each sample was identified using two approaches: (1) automatic decomposition of the age distribution into its component ages using the mixture-modeling approach of Galbraith (2005); (2) determining the minimum-age peak using only the ages younger than 20 Ma, in order to reduce the error on the minimum-age peak. Both methods are used as implemented in the Density Plotter software (Vermeesch, 2012). We use the resulting youngest age peaks to constrain the

maximum depositional age for each sample. As the AFT system is partially annealed at temperatures between *ca.* 60 to 120 °C (Gallagher and others, 1998), it is possible that the more deeply buried samples do not retain their pre-depositional age signal. We assess the possibility of post-depositional AFT annealing in our samples using the observed age-depth pattern (van der Beek and others, 2006; compare interpretation section).

Magnetostratigraphy.—Only the upper part of the Remi section has sufficient continuous exposure to allow meaningful magnetostratigraphic sampling and analysis. A total of 186 paleomagnetic sites were sampled at stratigraphic intervals of 5 to 6 meters on average, with some larger gaps due to the lack of exposure or unsuitable lithologies (weathered gravelly sandstone). Remanent magnetizations of samples were analyzed on a 2G Enterprises DC SQUID cryogenic magnetometer inside a magnetically shielded room, at the Geosciences Rennes paleomagnetic laboratory (France). Details of the sampling strategy and analysis are provided in Supplementary Materials 1 and 3 (http://earth.geology.yale.edu/%7eajs/SupplementaryData/2018/Govin).

Provenance Analysis

Zircon U-Pb geochronology.—U-Pb dating was carried out on detrital zircon cores and rim overgrowths from Sibo, Remi and Siang samples, in order to decipher the provenance of the deposits from these sections.

Nine medium- to coarse-grained samples were selected at regular stratigraphic intervals throughout the sections. One sample is from the Sibo outcrop, six are from the Remi section (fig. 3) and two from the Siang section. Remi samples have been analyzed for both zircon rims and cores, detected using cathodoluminescence imaging prior to analysis. For the Siang samples, we compare our data with that of Lang and Huntington (2014), who previously dated zircons from the Siang section using the U-Pb method. Zircon grains were separated and imaged at Lancaster University and at the NERC Isotope Geosciences Laboratory (NIGL, UK). Zircon U-Pb dating was performed at NIGL (UK) using a Nu Instruments AttoM single-collector inductively coupled plasma mass spectrometer (SC-ICP-MS). Several rim-dating methods were attempted; these are described in detail in Supplementary Materials 1. The analytical data, details of standard calibration and isotopic corrections, as well as screening procedures adopted, are presented in Supplementary Materials 5.

Apatite U-Pb geochronology.—The use of the LA-ICP-MS technique for AFT analyses has the advantage that it permits apatite U-Pb ages to be determined on the same grains in the same analytical session. A detailed description of the analytical procedure, age correction, and data processing is provided in Supplementary Materials 1 and 4. Apatite U-Pb age treatment followed the approach of Chew and others (2011), using an iterative approach to obtain a $^{207}Pb/^{206}Pb$ intercept value based on a starting estimate generated from the terrestrial Pb evolution model of Stacey and Kramers (1975). This was used to calculate a ^{207}Pb-corrected $^{238}U/^{206}Pb$ age. Since the ^{207}Pb-based correction assumes U-Pb* (radiogenic Pb) elemental concordance, which may not be the case for detrital grains, knowledge of likely source-area ages is required to discriminate partially reset ages in the same manner as for detrital AFT analysis. Additionally, as none of the apatite U-Pb analyses were concordant with respect to age, data screening was performed with a similar approach to that described by Zattin and others (2012) and Mark and others (2016). Apatite U-Pb results are discussed in the U-Pb geochronology section where they are compared with zircon U-Pb data.

RESULTS

Paleomagnetic and Luminescence Dating of the Siwalik Sediments at Sibo

The unconsolidated nature and gentle deformation of the Sibo outcrop suggests that these Upper Siwalik sediments are geologically young. The palaeomagnetic

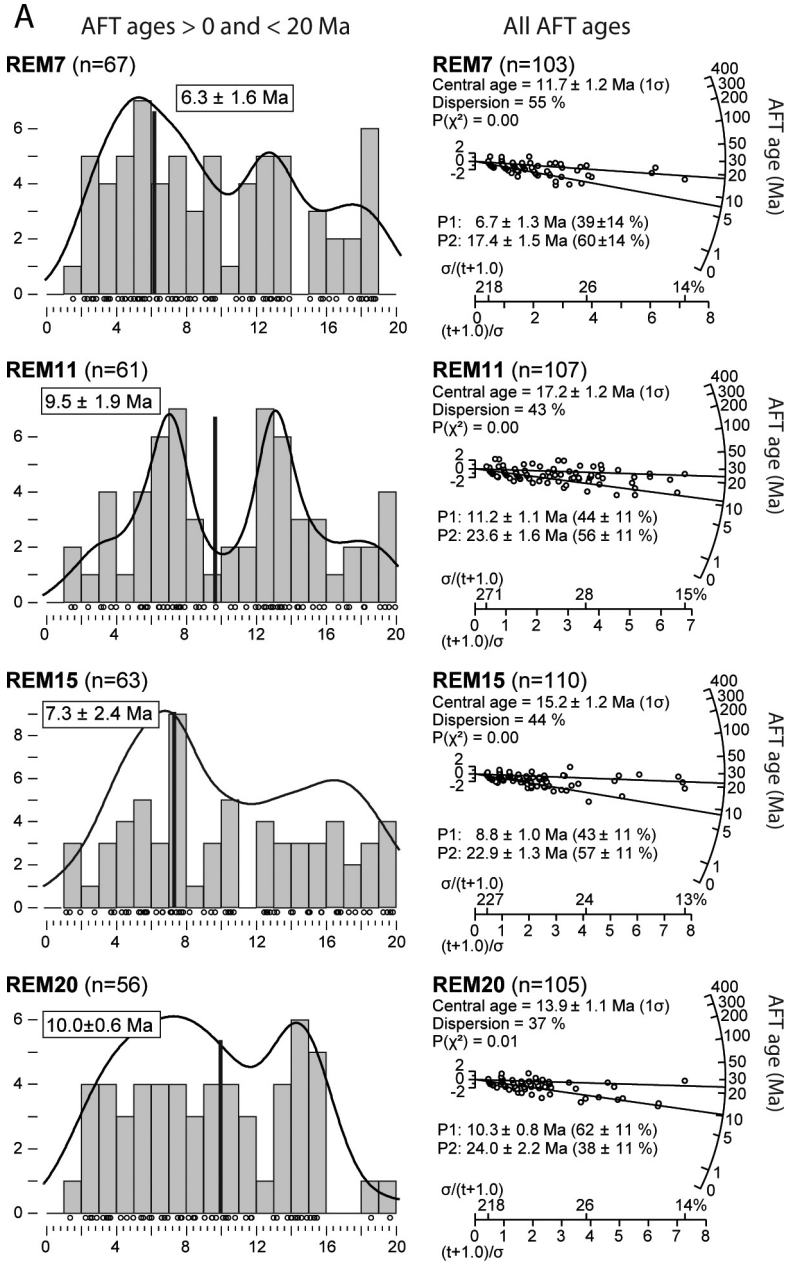

Fig. 4. Apatite fission-track data for samples from the Remi and Siang sections. The left column shows ages <20 Ma for each sample, plotted as adaptive Kernel density plots (Vermeesch, 2012) with overlying histograms; n=number of grains <20 Ma. Framed number shows the minimum age peak generated with Density Plotter program (Vermeesch, 2012). The right column shows AFT data reported in radial plots and considering the total number of dated grains in each sample, indicated next to sample name (n=X). The central age, dispersion, χ^2 probability and main peak ages (± 1σ, with percentages referring to the relative importance of each peak) are indicated.

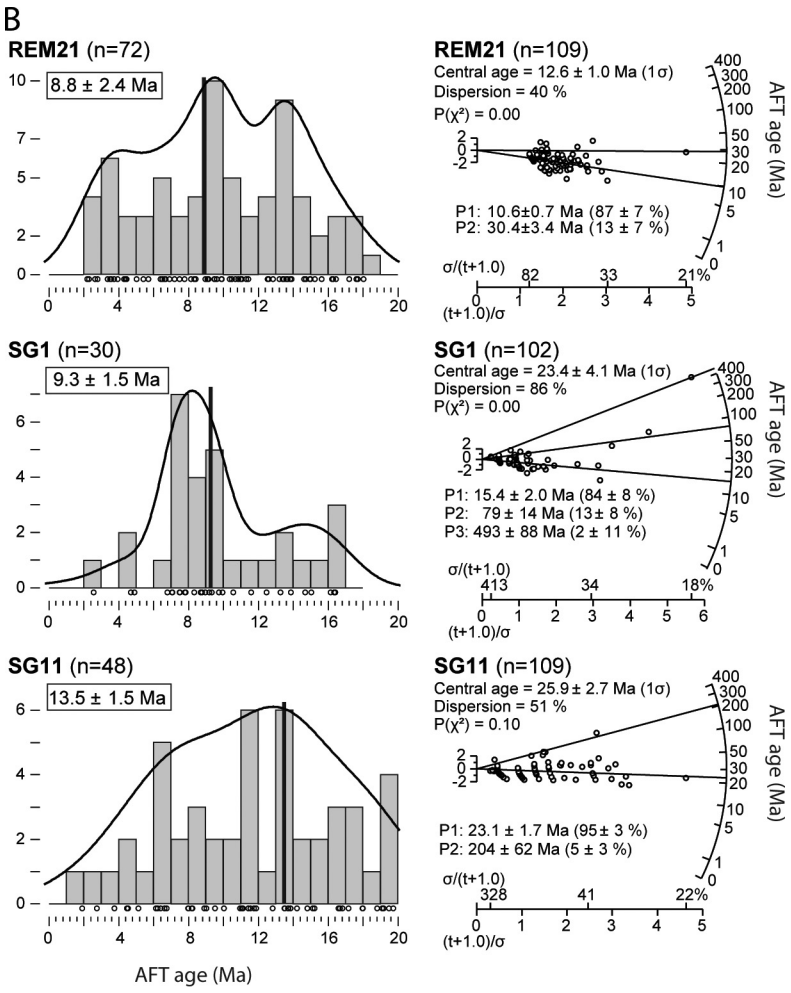

Fig. 4. (continued).

analysis (see Supplementary Material 3) yields stable Characteristic Remanent Magnetizations directions defined from 500 to 570 °C with a normal polarity orientation in both cores from the Sibo location. The dose-response curve for the IRSL data shows a saturation plateau reached at *ca.* 1.2 kGy and all D_e values range between 300 and 800 Gy (Supplementary Materials 1; fig. S1-1), resulting in a mean burial dose of 430 ± 21 Gy and an uncorrected IRSL date of 115 ± 11 ka (table S1). The D_e distribution shows measurements for the 28 aliquots describing 25 percent over-dispersion, similar to the samples from Abrahami and others (2018), suggesting partial bleaching is not a problem in these samples. Fading tests were relatively uniform and result in a mean g-value used for D_e correction of 4.73 ± 0.83 percent per decade. As the signal is too high on the dose-response curve to make a reliable correction for fading, the resulting corrected date of 190 ± 18 ka must be regarded as a minimum age.

Apatite Fission-Track Dating

AFT single-grain ages are reported in Supplementary Materials 4; data are shown in figure 4. Single-grain apatite fission-track ages range between 0 and >1000 Ma. All

samples contain considerable numbers (typically around 20, but up to 35 in SG1) of zero-track grains; REM samples contain 3 to 10 grains with pre-Himalayan (>50 Ma) dates, while samples SG1 and SG11 contain 11 to 15 of such grains. The minimum-age populations and P1 age peaks generated from our results are generally within error of each other, with the minimum age population typically somewhat younger (fig. 4). The SG samples form an exception to this, as the minimum-age population (calculated from grains <20 Ma) is significantly younger than the P1 age peak. The minimum ages also show overall younging from the supposedly stratigraphically lowest sample in the Siang section (SG11), with a minimum-age population of 13.5 ± 1.5 Ma, to the uppermost sample in the Remi section (REM7), with a minimum age population of 6.3 ± 1.6 Ma (fig. 4). There are a few exceptions to this trend, however, with samples REM11 and REM20 showing older minimum ages (but within error) than the samples that are stratigraphically below them.

Magnetostratigraphy

Magnetization characteristics.—The initial Natural Remanent Magnetization (NRM) intensities range from 10^{-5} to 10^{-1}A/m and generally increase up-section. This increase, also observed in the bulk susceptibility, likely reflects a higher concentration of strongly magnetic iron oxides, such as magnetite, in the upper levels of the section. Two clearly different thermal demagnetization behaviors, separated by the stratigraphic level 1200 m, represent a change in lithology, grain size, and demagnetization behavior. We used these behaviors to define Characteristic Remanent Magnetization (ChRM) components (fig. 5).

Demagnetizations from the lower part (below the 1200 m-level) were mainly complete below 550 °C (fig. 5C) and a viscous component often removed below 200 °C. A low-temperature component (LTC) of normal polarity, mostly demagnetized between 150 and 300 °C, was interpreted as an overprint. A medium-temperature component (MTC), generally demagnetized between 150 and 400 °C, often overlapped with the LTC along great circle paths on stereographic projections (see fig. S1-2 in Supplementary Materials 1). This MTC, of normal or reversed polarity directions, was interpreted as representing the ChRM. The increase in remanence intensity and susceptibility upon heating above *ca.* 300 °C is characteristic of iron sulphide transformation to magnetite as also observed in other sections from rocks of the eastern Himalayan Siwalik Group (Chirouze and others, 2012; Coutand and others, 2016).

Generally, samples yielded higher initial NRM intensities in the upper part of the section (above the 1200 m-level) than in the lower part of the section. However, the thermal demagnetization paths were more erratic and unstable, and many samples did not yield interpretable directions (figs. 5E and 5F). This is explained by the larger grain size of the upper part of the section (fig. 3), which yields multi-domain magnetic grains (Butler, 1992). Samples presenting interpretable demagnetization paths have generally much higher unblocking temperatures, between 300 and 670 °C, suggesting magnetite-like minerals and the occasional occurrence of hematite.

ChRM directions.—ChRM directions obtained from standard methods (see Supplementary Materials 1) were classified in four quality groups (fig. 5). Quality 1 (Q1) are well-defined directions determined from a stable linear demagnetization path of MAD <15° (figs. 5A and 5B). Quality 2 (Q2) have clearly defined polarities but less robust directions because of secondary overprint and/or directional scatter (figs. 5C and 5D). Quality 3 (Q3) have ambiguous polarities, usually due to a strong overprint and/or a weak scattered signal (figs. 5E and 5F). Also included in Q3 are poorly indurated samples that crumbled before sufficient measurements were acquired to extract reliable ChRM directions. Quality 4 (Q4) are Q1 or Q2 directions with Virtual Geomagnetic Poles (VGPs) lying more than 45° from the mean VGP (see fig. S1-3 in the Supplementary Material 1). This 45° cut-off procedure was performed separately

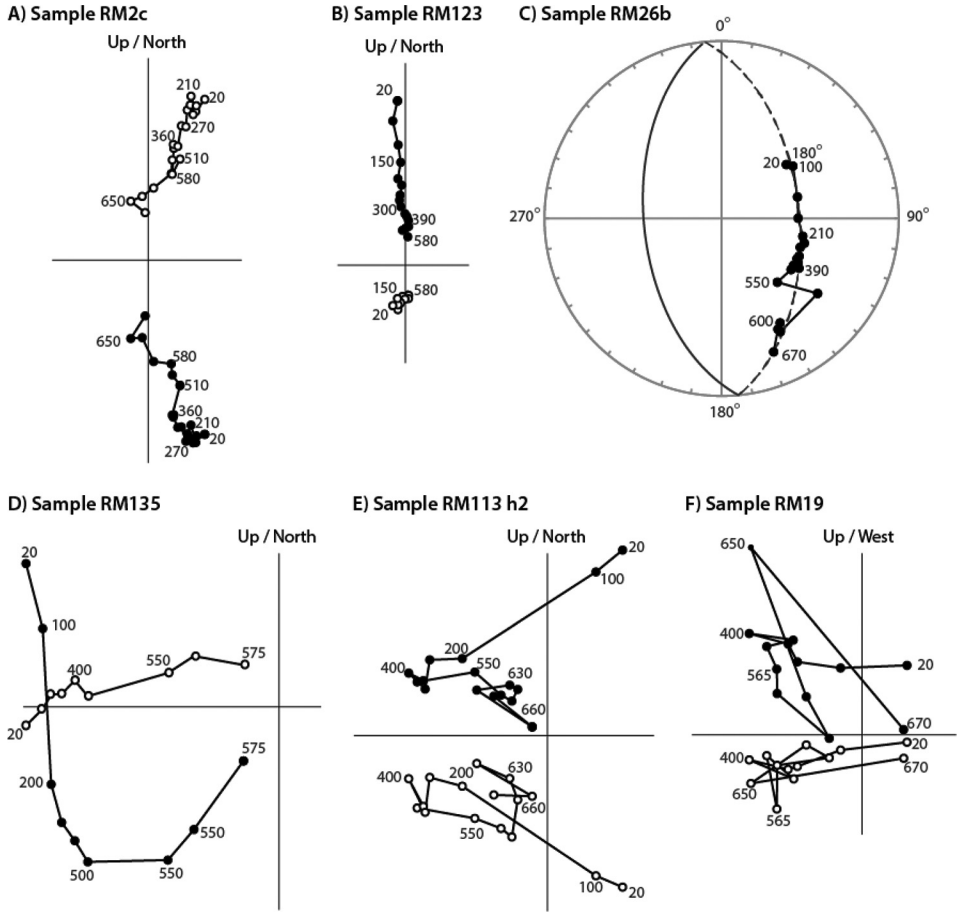

Fig. 5. Representative thermal demagnetization paths presented on vector-end point diagrams and stereographic projection (C). Full and open symbols are projections on the horizontal and vertical plane, respectively. The numbers next to the symbols indicate the temperature of the demagnetization step in °C. (A) and (B) are reliable directions and polarities from group Q1. (C) and (D) are reliable polarities but of less reliable directions from group Q2. (C) is a typical demagnetization path on which great-circle analysis was performed on a stereographic projection (McFadden and McElhinny, 1988). (E) and (F) are unreliable directions and polarities from group Q3. Figures were generated using Paleomagnetism.org (Koymans and others, 2016).

for normal and reversed polarity datasets to avoid introducing a bias. In total 25 Q1 and 54 Q2 directions were defined and used for further analyses, while Q3 and Q4 directions were systematically rejected.

These remaining Q1 and Q2 ChRM directions cluster in antipodal fashion after tilt correction indicating the section has not been fully remagnetized (compare fig. S1-2 in Supplementary Materials 1). A fold test was not applicable as the Remi section is homoclinally tilted. The reversal test is negative: the normal directions do not share a common true mean direction with the antipodal of the reversed directions (Koymans and others, 2016). This is expected with data that include partial normal overprints affecting both normal and reversed directions. In this case, reverse polarity determinations are clearly reliable but normal polarities may result from a total overprint of an original reverse direction, despite the care taken in isolating ChRM directions. For this

reason, we have been especially cautious in defining normal polarities. This is critical in the upper part of the section, where commonly unstable demagnetization yielded non-consecutive normal polarity directions. These included originally reversed directions with normal secondary overprints extending to high temperature ranges, suggesting some other samples may be fully remagnetized into normal polarities. In the lower part of the section, however, normal polarities were usually well defined by higher-temperature linear demagnetization paths and observed in consecutive intervals, validating normal-polarity zones. Nevertheless, we present the normal-polarity intervals as not fully reliable throughout the section to convey the possibility of normal overprints into the record.

The remaining 79 ChRM directions from Q1 and Q2 groups thus provide paleomagnetic polarity determinations at intervals averaging 13.6 m throughout the Remi section (fig. 3). Several larger gaps could not be avoided due to lack of exposure or inadequate rock type preventing sampling, or samples yielding non-interpretable demagnetization paths. To define polarity zones, isolated polarities were systematically rejected. We thus identified two normal polarity (N1 and N2) and three reverse (R1, R2 and R3) zones in the section (fig. 3). The upper part of the magnetostratigraphic section shows a significant number of isolated normal polarity directions. Because these are isolated and they occur in the coarser-grained part of the sedimentary section where normal overprinting is common, they are considered unreliable. However, it is possible that these isolated normal polarity sites reflect original normal polarity zones that are not confidently deciphered by our results.

U-Pb Zircon and Apatite Geochronology

U-Pb zircon cores.—Between 32 and 116 zircons from each analyzed sample have U-Pb dates of acceptable quality (fig. 6; screening criteria are summarized in Supplementary Materials 1 table S1-3, and Concordia plots are shown in Supplementary Materials 1 fig. S1-4). Throughout the combined section, dates range between 21 and 3054 Ma. All samples contain a significant proportion of zircons with ages $<$300 Ma (between 12% and 54%); within this age range, grains are mainly of Late Cretaceous-Early Paleogene age (40–100 Ma), with a few zircons younger than 40 Ma, and most samples contain a few zircons of Early Cretaceous age (100–140 Ma). The main population of $>$300 Ma zircons is Paleozoic in age, defining a major peak at around 500 Ma, with two subordinate populations with Proterozoic ages, around 900 and 1600 Ma. From the Siang, through the Remi to the Sibo locations there is a well-defined trend of increasing proportions of older (Paleozoic and older) grains, particularly the 500 Ma population, at the expense of the Cretaceous-Paleogene population (fig. 7). The clearest shift in this trend occurs within the Remi section, between samples REM21 and REM15, with sample REM20 transitional between the two.

U-Pb zircon rims.—U-Pb zircon-rim ages with $<$5 percent discordance range from 16 to 3704 Ma (fig. 6). If grains with a higher discordance percentage are included, the results present a few ages as young as 15.2$\pm$0.4 Ma (6.5% discordant, in sample REM3) for age discordance limited to 10 percent, and as young as 5.1$\pm$0.2 Ma (55.5%

Fig. 6. U-Pb zircon and apatite data for samples from the Sibo, Remi, and Siang sections and from modern riverbeds compared to potential source regions. Data are plotted as kernel density plots (Vermeesch, 2012). Data from this study are plotted in blue for zircon and red for apatite. n=x indicates the number of grains yielding acceptable U-Pb ages (see Supplementary Methods for details of data treatment). Zircon U-Pb source-area compilation: ages of zircons characteristic of Greater, Lesser and Tethyan Himalayan source units, all from Gehrels and others (2008) and references therein, Gangdese from Ji and others (2009), and Bomi-Chayu ages from references in Lang and Huntington (2014). The top graph presents data from modern riverbeds, the Lohit River ages (Cina and others, 2009) are presented in dashed line and the Siang River ages (Lang and others, 2013) with solid line. Depositional ages of samples determined in this study are shown to the left of the plots.

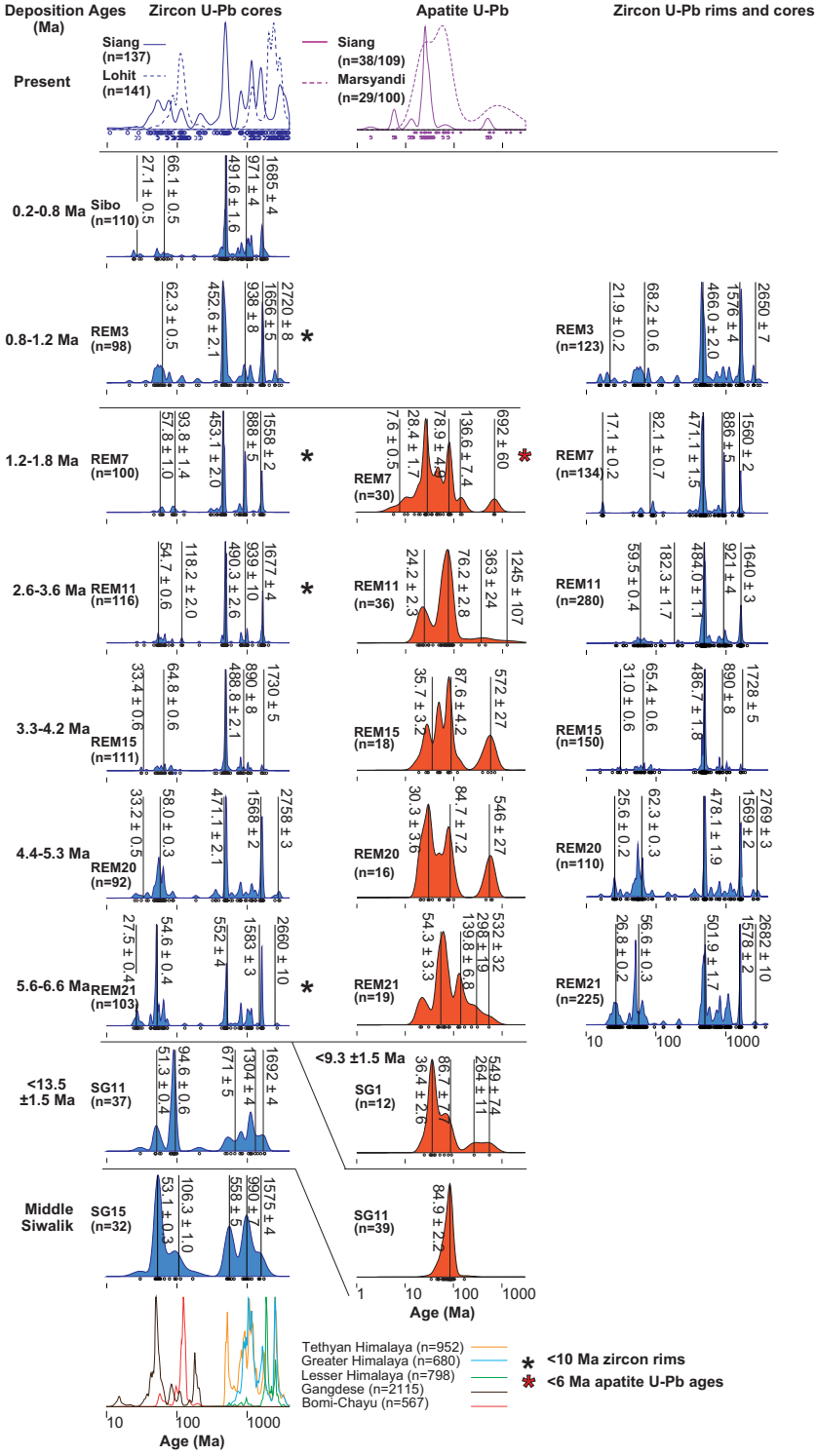
Deposition Ages (Ma)
Zircon U-Pb cores
Apatite U-Pb
Zircon U-Pb rims and cores
Present
Siang (n=137)
Lohit (n=141)
Siang (n=38/109)
Marsyandi (n=29/100)
0.2-0.8 Ma
Sibo (n=110)
0.8-1.2 Ma
REM3 (n=98)
REM3 (n=123)
1.2-1.8 Ma
REM7 (n=100)
REM7 (n=30)
REM7 (n=134)
2.6-3.6 Ma
REM11 (n=116)
REM11 (n=36)
REM11 (n=280)
3.3-4.2 Ma
REM15 (n=111)
REM15 (n=18)
REM15 (n=150)
4.4-5.3 Ma
REM20 (n=92)
REM20 (n=16)
REM20 (n=110)
5.6-6.6 Ma
REM21 (n=103)
REM21 (n=19)
REM21 (n=225)
<13.5 ±1.5 Ma
SG11 (n=37)
<9.3 ±1.5 Ma
SG1 (n=12)
Middle Siwalik
SG15 (n=32)
SG11 (n=39)
Age (Ma)
Tethyan Himalaya (n=952)
Greater Himalaya (n=680)
Lesser Himalaya (n=798)
Gangdese (n=2115)
Bomi-Chayu (n=567)
<10 Ma zircon rims
<6 Ma apatite U-Pb ages

Fig. 6

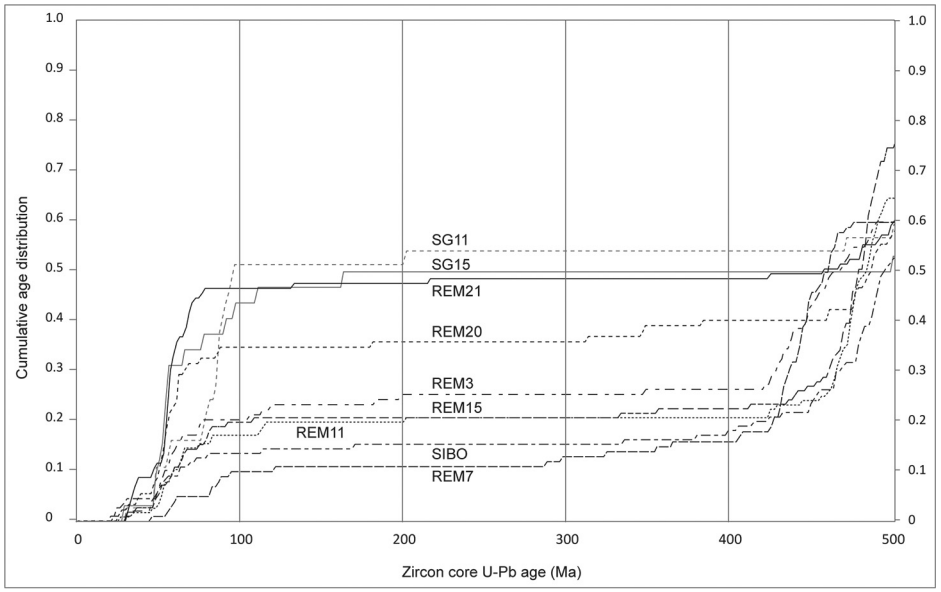

Fig. 7. Cumulative age distribution of zircon U-Pb data. The trend of increasing ~500 Ma grains at the expense of arc-aged (Mesozoic-Paleogene) zircons is observed up-section, with the greatest change between REM21 and REM15, with REM20 as a transitional sample.

discordant, in sample REM7) with no discordance limit on the data (fig. 6 and Supplementary Materials 1, table S1-4). The stratigraphically lowest sample to contain rim ages of 10 Ma or less, without discordance distinction, is REM21. Concordia diagrams of the rim analyses showing ages ≤20 Ma are plotted in Supplementary Materials 1, figure S1-5. The youngest lower intercept of the discordia line with the concordia curve calculated from several analyses of the same rim is 8.5±1.9 Ma (MSDW=3.00) in sample REM11.

A total of 24 rim analyses yielded ages between *ca.* 33.4 to 15.2 Ma, and Th/U ratios <0.1, typically considered to indicate a metamorphic origin (for example, Hoskin and Schaltegger, 2003). These young metamorphic rims are present in every sample for which rim analyses were carried out, except REM20. In addition, two core analyses yielding Oligo-Miocene ages and metamorphic Th/U ratios were obtained from REM21.

Apatite U-Pb Geochronology

We obtained between 13 to 37 acceptable U-Pb ages per sample, ranging between 5 and 1635 Ma. The relatively small total populations do not reflect a paucity of apatite; 110 successful ablations of stoichiometric apatite were carried out for each sample, but the typically high levels of common-Pb (that is Pb not produced by *in-situ* radioactive decay) meant that most grains yielded ages associated with unacceptably high uncertainty. The Cretaceous-Cenozoic age populations identified using apatite U-Pb dating are similar to those observed using zircon U-Pb dating; pre-Cretaceous ages are only sparsely represented in the apatite U-Pb data, reflecting the highly refractory nature of the U-Pb system in zircon. The main age peaks and the age distributions follow a similar trend in both datasets, being dominated by ages between *ca.* 40 to 110 Ma (fig. 6). Although the temperature sensitivity (assuming thermally-activated volume diffusion) of these two geochronological systems differ by several hundred °C (U-Pb apatite

temperature sensitivity of *ca.* 375 to 550 °C; zircon >900 °C; Cherniak and Watson, 2000; Schmitz and Bowring, 2003 and references therein; Cochrane and others, 2014), the respective Cretaceous-Cenozoic age populations broadly match, suggesting age spectra are dominated by igneous crystallization ages. There is a sharp change in apatite U-Pb spectra between SG11 and SG1: SG1 and subsequently-deposited samples all yield numerous apatite U-Pb ages < 40 Ma, but SG11 yields only a single grain of this age. We caution however that this shift is defined only by a single sample, SG11.

Few apatite grains are of Early Cretaceous age, and these are exclusively from samples that also contain zircons of this age, strongly indicating an igneous source for these grains, as opposed to metamorphic resetting of the more thermally sensitive apatite U-Pb system. We also note the occurrence of very young apatite U-Pb ages in sample REM7 of 5.7 ± 0.5 and 9.5 ± 0.8 Ma.

The paucity of extremely young AFT ages (<1 Ma), as reported for other detrital thermochronometric techniques applied to modern sediment draining the syntaxis (for example, Bracciali and others, 2016), may appear surprising given the low temperatures to which the fission track system in apatite is sensitive. However, the relatively low U content typically found in apatite increases the likelihood that for a grain which has cooled recently either (1) a fission event will not occur, or (2) will not be observed during counting, given that in data governed by Poissonian statistics such as FT, an observation of zero implies a true value of between 0 to 3. This problem is acute in detrital analysis, where grains may not meaningfully be pooled as multiple source populations are present (in contrast to bedrock samples). Supplementary Material figure 4b illustrates that the lower the U content, the older are the youngest AFT ages observed. This observation has two implications: (1) our minimum AFT ages, used to characterize deposition age, may substantially over-estimate the maximum age of deposition; and (2) detrital AFT may be an inappropriate technique for the detection of terranes which have cooled extremely recently (<1 Ma).

DISCUSSION

Depositional Age of the Sibo, Remi, and Siang Successions

The IRSL and palaeomagnetic results, AFT ages and the magnetostratigraphic analysis, along with the field observations, allowed us to constrain the depositional ages of parts of the sedimentary sections and to propose an age model for the Sibo, Remi, and Siang successions.

Constraints from IRSL and paleomagnetic data.—The unconsolidated nature and gentle deformation of the Sibo outcrop suggests that these Upper Siwalik sediments are significantly younger than the top of the Remi section. The IRSL data constrain the minimum age of the rocks at *ca.* 190 ka, whereas the measured normal paleomagnetic polarity, limits the maximum age of the Sibo sediments to the C1n Brunhes chron (Middle-Late Pleistocene; < 770 ka) or possibly short older chrons within C1r (Matuyama; C1r.1n, C1r.2n), both <1.2 Ma (Gradstein and others, 2012). However, the incomplete saturation of the IRSL signal indicates that an age closer to the minimum (that is during the Brunhes chron) is more likely. The depositional age of the Upper Siwalik sediments at Sibo is therefore roughly constrained to 480 ± 290 ka. These sediments have subsequently been gently tilted by the active Main Frontal Thrust, associated with southward propagation of the Himalayan front (for example, Srivastava and others, 2009).

Constraints from AFT ages.—For the Remi and Siang sections, AFT ages can provide initial constraints on depositional age if they are not reset by burial heating. Apatites anneal at different temperatures, depending on their chemistry (for example, Carlson and others, 1999), and it is possible that partially reset ages are present in our data. To investigate this possibility, we first review burial estimates from other Siwalik sections.

Vitrinite reflectance data and illite crystallinity analyses from Siwalik sections in Nepal indicate maximum temperature-depth couples that imply a geothermal gradient of 18 to 24 °C/km, consistent with well data in western India, and leading to partial resetting of the AFT system at burial depths greater than ~2500 m (for example, Huyghe and others, 2005; van der Beek and others, 2006). Similar results were obtained in the Kameng section of western Arunachal Pradesh (Chirouze and others, 2013). In the 2200 m thick Dungsam Chu section (Bhutan), the maximum burial temperature determined with vitrinite reflectance is 80 °C and AFT ages are unreset throughout the section (Coutand and others, 2016). The Remi section is only *ca.* 1900 m thick, but estimating the initial maximum thickness of the Siang section is not straightforward because the upper part of the sedimentary pile does not crop out at present. Additionally, thrusts both within and bounding the Siang and Remi sections (for example Sompa Fault, Mingo Thrust; fig. 2) could have buried parts of the sections significantly deeper than the stratigraphic depth, rendering the maximum depth and temperature difficult to estimate. However, since minimum apatite fission-track ages young upward in both the Remi and Siang sections, we interpret these ages as unreset, or at most slightly partially reset due to potential post-depositional burial heating. Thus, we consider the minimum AFT age-peak as the maximum depositional age for each sample in the Remi and the Siang sections.

We conclude that the Middle and Upper Siwalik rocks in the Remi section were deposited after 8.8 ± 2.4 (REM21) to 6.3 ± 1.6 (REM7) Ma. In the Siang section, SG11 was deposited after 13.5 ± 1.5 Ma and SG1 after 9.3 ± 1.5 Ma (fig. 6).

Constraints from magnetostratigraphy.—For the Remi section, further age control is provided by correlating our magnetostratigraphic results to the Geomagnetic Polarity Time Scale (GPTS; Gradstein and others, 2012). As a starting point of our correlation we use the reverse zone R2 as it is the most clearly defined with its basal reversal located within the more reliable lower part of the section. Five stratigraphic levels are assigned a maximum depositional age determined using the independent constraints provided by the detrital apatite fission-track dating (fig. 4). In particular, the stratigraphic age at the base of the Remi paleomagnetic section, in the reverse zone R3, is $<7.3 \pm 2.4$ Ma (fig. 3). This age constraint yields four possibilities for correlating R2 to the GPTS: A) to *C3r* (starting at 6.0 and ending at 5.2 Ma), B) to *C2Ar* (4.2 to 3.6 Ma), C) to the combination of *C2r.3r* to *C2r.1r* (2.6 to 1.9 Ma); and D) to *C1r* (1.8–0.8 Ma; fig. 3).

Correlation A links R3 to the oldest reverse chron *C3Ar* allowed by the AFT-derived maximum depositional age; the overlying N1 matches chron *C3n.4n.* The lengths of the N1, R2 and N2 zones relative to each other suggest that N2 is correlated to the chrons *C3n.1n* to *C3n.2n*, implying a missing reverse polarity zone within N2, which would be possible considering the gap and reverse isolated site within N2. The correlation is not straightforward, however. We can speculatively correlate the normal isolated polarities within R2 to the interval from *C3n.3r* to sometime in *C2Ar*, which includes relatively short normal chrons (*C3n.1n, C3n.2n and C3n.3n*).

In correlation B, R2 is correlated to *C2Ar.* This implies N2 to correspond with the chrons from *C3n.1n* to *C3n.4n* and the subsequent R3 zone to *C3r.* This would imply missing polarity zones *C3n.1r, C3n.2r* and *C3n.3r*, which would represent a significant amount of missed reverse polarity directions, possibly due to secondary overprinting. Above R2, N1 is logically correlated to *C2An.3n*, but R1 is too long to be realistically correlated to *C2An.2r.* This correlation would imply a very significant number of missing polarity zones, reverse in the lower part of the section and normal in the upper part.

In correlation C, correlating R2 with the *C2r.1r* to *C2r.3r* interval implies that the two very short normal zones of the GPTS within this time interval (Réunion events) are missing in our data. Below R2, the correspondence of N2 to the chrons from *C2An.1n*

to *C2An.3n* is straightforward, although it implies that the isolated reverse direction site and the sampling gap within N2 respectively reflect and hide the missing chrons *C2An.1r* and *C2An.2r*. Below N2, R3 is easily linked to *C2Ar*. Above R2, the long reverse zone R1 fits well with the *C1r.2r to C1r.1R* reverse chrons. However, the correlation of the top of R1 becomes challenging to interpret with numerous options. These are based on assumptions made on the isolated normal sites, which could independently reflect original normal polarities or result from secondary overprinting. Since the potential solutions are multiple, they are not detailed here. However, as the top of the section clearly indicates a reverse polarity zone, it must be older than *C1n,* that is the Brunhes-Matuyama boundary, *ca.* 0.8 Ma.

In the youngest correlation D the normal zone N2 is assigned to chron *C2n* (Olduvai). The underlying reverse zone R3 would thereby correlate to chron *C2n.1r*, putting the age of the base of the Remi section at slightly over 2 Ma. The section top must also be older than the Brunhes-Matuyama boundary, *ca.* 0.8 Ma but could be as old as 1.1 Ma depending on whether the C1r.1n (Jaramillo) chron has been missed. Correlation D would imply that the large zone N1 is a remagnetization artefact and necessitates very large accumulation rates of *ca.* 1 m/kyr throughout the section.

Correlations A, B and D are not as straightforward as correlation C based on paleomagnetic considerations alone. Correlations A, D and especially B require more assumptions on missed intervals, remagnetizations, gaps, accumulation rates, and fitting isolated polarities. In contrast, correlation C provides the best fit to the polarity timescale while omitting the fewest number of chrons. We therefore prefer this correlation and infer the base of the magnetostratigraphically dated part of the Remi section to be younger than 4.2 Ma. The Middle to Upper Siwalik boundary in the Remi section is constrained at *ca.* 2.5 Ma.

Comparison to other eastern Himalayan sections.—We note that the preferred correlations C (and more dramatically D) implies that AFT lag times (that is, the difference between minimum AFT ages and depositional ages) are much longer in the Remi section (of the order of 4–6 Myr) than elsewhere in the Sub-Himalaya, where they are typically <2 Myr (van der Beek and others, 2006; Chirouze and others, 2013). However, correlation A and B places the Middle to Upper Siwalik transition at *ca.* 5.5 Ma and 4.2 Ma respectively, whereas it has been dated between 2 and 3.8 Ma throughout the Himalayan sections from Pakistan to eastern India (for example, Sanyal and others, 2004; Ojha and others, 2009; Chirouze and others, 2012; Coutand and others, 2016) and <2 Ma in the nearby Siji section (fig. 8; Lang and others, 2016).

Given the apparently long AFT lag times noted above, the minimum AFT ages in samples REM20, REM21, SG1 and SG11 only provide limited constraints on the depositional ages of these samples. However, their lithology clearly identifies these samples as Middle Siwalik rocks; Lower Siwalik rocks were nowhere encountered in the investigated successions or the nearby Siji section. The Lower to Middle Siwalik boundary is generally dated around 10 Ma along the Himalayan foreland basin (Johnson and others, 1985; Harrison and others, 1993; Meigs and others, 1995; Gautam and Fujiwara, 2000; Ojha and others, 2000, 2009; Chirouze and others, 2012), with the notable exception of Coutand and others (2016) who placed the boundary *ca.* 6 Ma in Bhutan (Dungsam Chu section). The oldest dated Lower to Middle Siwalik transition has been constrained at *ca.* 11 Ma (Johnson and others, 1985; Ojha and others, 2000, 2009) in the Chinji, Khutia Khola and Tinau Khola sections of Pakistan and Nepal. Therefore, we conservatively assume that the oldest Middle Siwalik sedimentary rocks of the Remi and Siang sections are ≤11 Ma, which is consistent with the AFT minimum age of 13.5 ± 1.5 Ma for the stratigraphically lowest analyzed sample SG11.

The section nearest to ours is the Siji River section located ~50 km west-southwest of the Remi River (fig. 1). Considering the age constraints, these two sections partly

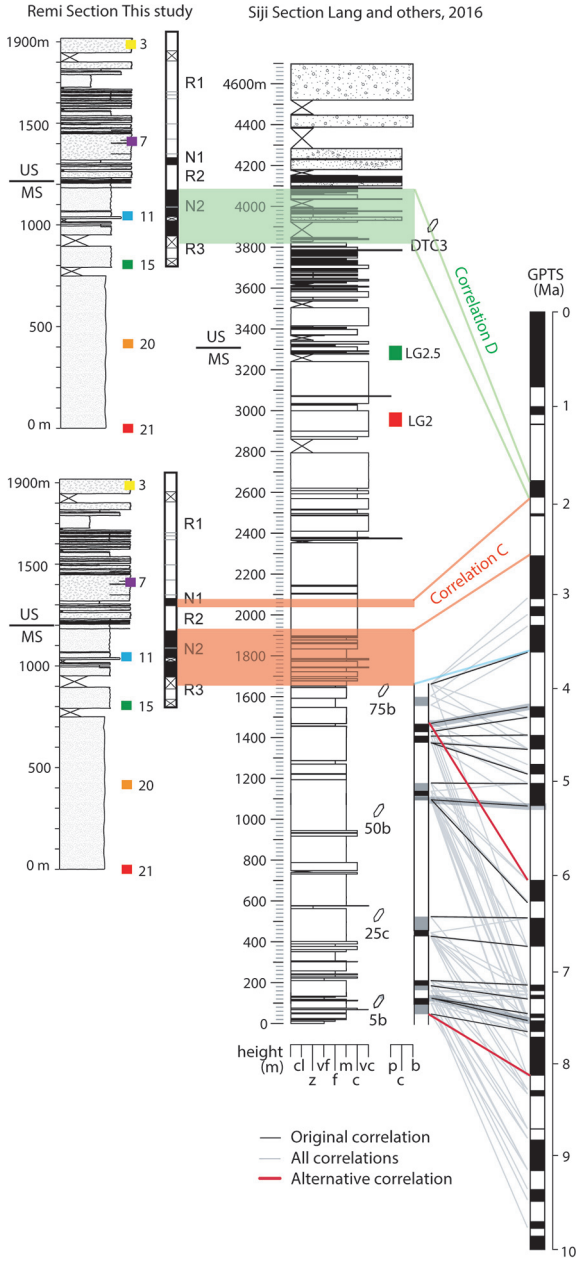

Fig 8. Comparison of the Remi section to the Siji section reported by Lang and others (2016) located *ca.* 50 km to the southwest (see fig. 5a in Lang and others, 2016). For the Remi section, two stratigraphic positions are represented according to correlation C (preferred) and correlation D to the Geomagnetic Polarity Time Scale (GPTS). Provenance samples are indicated by colored squares with associated sample numbers. For the Siji section, red bars indicate alternative correlation (see text). Samples LG2.5 and LG2 record similar provenance change as samples REM15 and REM21 from the Remi section. DTC3 has a maximum depositional age estimated within 1-2 Ma (see Lang and others, 2016). Upper Siwalik (US) to Middle Siwalik (MS) boundaries are indicated according to the litho-stratigraphic interpretations of the respective studies.

overlap in time, with the magnetostratigraphically-dated part of the Remi section (correlation C) from chrons *C4n.1r* (3.8 Ma) to *C2Ar* (*ca.* 1 Ma) being younger than the magnetostratigraphically-dated part of the Siji section from chrons *C4n.1r* (7.6 Ma) to *C2Ar* (3.5 Ma). Based on these constraints, however, the Middle to Upper Siwalik transition occurs diachronously at 2.4 Ma at Remi and <2 Ma at Siji. In addition, similar changes in U-Pb derived provenance recorded in both sections (see below) would also occur earlier at Remi and later at Siji. Although the Middle-Upper Siwalik boundary represents a facies transition that does not need to be synchronous, a synchronicity in the records of U-Pb derived provenance is expected if they resulted from deposition by the same trunk river system (that is, the Brahmaputra). Such synchronicity would require either much younger depositional ages of the Remi deposits (following the rejected correlation D) or older depositional ages of the Siji deposits, implying reconsideration of its magnetostratigraphic correlation. An alternative correlation may be found by placing the top of the dated part of the Siji section within chron *C3r*, at ~5.5 Ma, and its base within chron *C4n.2r*, at ~8.2 Ma (fig. 8). Although this correlation introduces a much larger variation in accumulation rates for the dated part of the section than the preferred correlation of Lang and others (2016), it renders the observed changes in provenance nearly synchronous between the Remi and Siji sections. We note that the correlation of Lang and others (2016) requires sedimentation rates to approximately double above the dated part of the Siji section, to accommodate the 2200 m of section between the top of the dated part (3.5 Ma) and sample DTC3, inferred to have a depositional age between 1 and 2 Ma (Lang and others, 2016). The alternative correlation would alleviate this problem.

Interpretation of Provenance and its Temporal Variations

By comparison with source regions (fig. 6, basal panel) we conclude that the Mesozoic-Early Paleogene zircon population recorded in the Siwalik rocks under study is derived from the Southern Asian margin. We suggest that the dominant ~50 Ma peak and paucity of grains >100 Ma indicates derivation from the Transhimalaya west of the syntaxis, rather than from more easterly equivalents. The Palaeozoic-Precambrian population can be derived from both the Lhasa Block and/or the Indian plate. We consider the 500-Ma peak as most likely derived from the Greater and/or Tethyan Himalaya, since this population is considerable in these two units whilst it is subordinate in the Lhasa block and lacking in the Lesser Himalaya. This inference is consistent with data from the Lohit River, which drains the Lhasa block but not the Tethyan or Greater Himalaya (fig. 1), and contains no 500 Ma zircons (Cina and others, 2009; Zhang and others, 2012). Interestingly, the 2500 Ma age peak, common to all units of the Indian plate, is absent in the Siwalik rocks under study. Likewise, the ~1800 Ma peak typical of the Lesser Himalaya is also absent from the Siwalik rocks of the Remi and Siang successions. Neogene zircons, predominantly rim ages, are recorded sporadically throughout the section. Their low Th/U values are suggestive of derivation from leucogranites of either the Greater Himalaya or Tethyan gneiss domes, rather than the Gangdese arc (Ji and others, 2009; Liu and others, 2016; Huang and others, 2017).

Sediment collected from rivers draining the modern syntaxis are characterized by zircon ages <10 Ma, and rutile and apatite U-Pb ages <6 to 5 Ma (Bracciali and others, 2016; Najman and others, in review[2]). No ages <10 Ma were obtained by this study using conventional spot analyses of zircon. We do report zircon rims <10 Ma, and also two apatite grains yielding U-Pb ages <10 Ma. These may be derived from the syntaxis

[2] Najman, Y., Mark, C., Barfod, D., Carter, A., Parrish, R., Chew, D., and Gemignani, L., Spatial and temporal trends in exhumation of the Eastern Himalaya and syntaxis as determined from a multi-technique detrital thermochronological study of the Bengal Fan: Geological Society of America Bulletin, in review.

(Bracciali and others, 2015) but could potentially also be derived from the MCT Zone (Braden and others, 2018).

Similar to the provenance interpretations for zircon U-Pb data, apatites of the dominant population with U-Pb age range *ca.* 54 to 87 Ma are interpreted as Transhimalayan-derived. Apatites in the population ranging from *ca.* 36 to 24 Ma are consistent with a Greater Himalayan source (Turab and others, 2017) or potentially derivation from the Tethyan leucogranites and gneiss domes. Derivation from the Transhimalya is considered unlikely in view of the lack of similarly aged zircons considered to be Transhimalayan-derived in the rocks under study. The decrease in age of this youngest apatite U-Pb population upsection (from 23 Ma in SG11 to 10 Ma in REM20; fig. 6) attests to the progressive exhumation of this source region.

The presence of Transhimalayan detritus from west of the syntaxis indicates derivation from the paleo-Brahmaputra river. Earlier suggestions that Transhimalayan material might have been deposited to the foreland basin via a transverse river draining from the Yarlung suture zone to the foreland basin in this area (Cina and others, 2009) is refuted by the discovery of Transhimalayan material in the foreland basin eastward and upstream of the proposed entry point of the putative transverse river (Lang and Huntington, 2014; this study).

A trend of increasing Indian-plate derived zircons (indicated in particular by the 500 Ma peak characteristic of the Tethyan and Greater Himalaya), at the expense of decreasing Transhimalayan input, is seen from the Siang to the Remi and the Sibo sections, with the major change occurring between samples REM21 and REM15 (>4.2 Ma). The trend is also observed in the Siang data of Lang and Huntington (2014); however, the exact percentages of such grains are not comparable between the two studies, probably due to different data-processing criteria. A similar decrease in arc-aged grains is seen between samples LG2 and LG2.5 in the Siji section downstream (Lang and Huntington, 2014), that is <3.5 Ma (Lang and others, 2016).

We discuss below the possible scenarios that may have resulted in this change. When considering these options, it is important to note the uncertainty in the palaeo-location of our sections with respect to the trunk paleo-Brahmaputra and its eastern and western tributaries, draining the Indo-Burman Ranges and Indian-plate Himalaya, respectively.

Dilution of the arc-derived signal by the rising Namche Barwa.—This hypothesis assumes the sections under study to be deposited by the trunk paleo-Brahmaputra, rather than eastern tributaries, which, as we have argued above, is the case based on the prominence of the 50 Ma zircon population and paucity of Early-Cretaceous grains. Support for the hypothesis that the observed trend is driven by the rising Namche Barwa massif (composed of Tethyan and Greater Himalayan rocks) comes from the record of short thermochronological (zircon fission-track and mica Ar-Ar) lag times, observed from 6 Ma onward in the Siji section (Lang and others, 2016) and from sample SG1 (<9.3 Ma) in the Siang and Remi sections (Govin, ms, 2017). These short lag times are interpreted as due to initiation of rapid exhumation of the syntaxial massif, and predate the time of the major decrease in arc-derived zircons by a few million years. A time-lag between the onset of short lag times and the decrease in arc-derived detritus can be explained if the Namche Barwa was exhumed from under a carapace of Transhimalayan arc material, as suggested for the Nanga Parbat massif in the western syntaxis (Najman and others, 2003; Chirouze and others, 2015). However, the change in provenance does not appear coeval between the Remi and Siji sections, which one would expect if the rocks from both sections were deposited by the same trunk river. The apparent lack of synchronicity between the Remi and Siji sections can be alleviated by a modified magnetostratigraphic correlation as discussed above (fig. 8), which would place the time of decreasing arc provenance in the Siji section at <5.5 Ma.

Dilution of the arc-derived provenance signal due to southward propagation of the thrust belt.—In this scenario, the Indian-plate detritus responsible for diluting the arc-derived provenance signal is delivered by transverse rivers, that is, westerly tributaries of the Brahmaputra. In the eastern Himalaya, south of the MCT, 500 Ma zircon U-Pb populations have been recorded in the Rupa Group (considered to be part of the THS) and the Miri Formation of the Gondwana Group (DeCelles and others, 2016). The Rupa Formation forms the hanging wall of the Bome Thrust, along with the Paleoproterozoic Lesser Himalayan Bomdila Group. The Gondwana Group comprises the hanging wall of the MBT. There is relatively little information available on the timing of movement on these thrusts. The Lesser Himalayan duplex is thought to have initiated around 10 to 12 Ma in Bhutan (Long and others, 2012), too early for the change we observe in the Remi section and also not associated with any increase, or indeed presence, of Paleoproterozoic Lesser Himalayan-aged grains that would accompany such a contribution. However, movement on the MBT, active at least in part at $<$7.5 Ma in the region (DeCelles and others, 2016), could have resulted in an increase in the 500 Ma population without a concomitant increase in Paleoproterozoic grains, through derivation from the Gondwana rocks. In this case, the difference in the time of the dilution of the arc-aged grains between the Remi and the Siji sections could be ascribed to delivery from different transverse rivers established at different times, or to along strike variation in the onset of thrusting along the MBT. A major cross-strike structure does exist between the two areas; it would thus be plausible that their tectonics differed.

We have reservations regarding this scenario to explain the data, however, since the paucity of zircons with ages characteristic of the Lesser Himalaya suggests only limited contribution of transverse rivers to the sediments. Nevertheless, we may ascribe some aspects of the provenance changes we see to southward propagation of thrusting. The trend of an upward-decreasing proportion of arc-derived grains is interrupted by sample REM 3 (fig. 7), which may have been partially recycled from the older Siwalik rocks. If this is the case, a reasonable explanation for such a recycled Siwalik component could be the onset of deformation in the Siwalik section of the Remi River between deposition of REM7 (*ca.* 1.5 Ma) and REM3 ($>$0.8 Ma), possibly through activation of the Mingo Thrust (fig. 2). The onset of activity on the Main Frontal Thrust was estimated at $<$1 Ma in the Kameng section, with activation of an internal Sub-Himalayan thrust (the Tipi Thrust) at *ca.* 1 Ma (Chirouze and others, 2013). Recycling and sedimentation during thrusting, as evidenced by growth strata in Upper Siwalik rocks, is also discussed for the Siji section (Lang and others, 2016). This scenario appears consistent with the proposed evolution in the Remi section, in which recycling was caused by initiation of the Mingo Thrust between *ca.* 1.5 and 1 Ma. This is also consistent with the observed transition to more proximal environments in the Upper Siwalik facies.

Change in drainage routing.—It has previously been proposed that the Yarlung may have originally connected to the Brahmaputra via the Lohit, prior to headward incision and capture by the Siang (for example, Robinson and others, 2014). Since the Lohit River lies east of the syntaxis, it does not traverse Greater or Tethyan Himalayan units (for example, see geological map in Zeitler and others, 2014), as evidenced by the paucity of 500 Ma zircons in its modern sediments (Cina and others, 2009; Zhang and others, 2012; fig. 6). Thus the time of any rerouting of the Yarlung-Brahmaputra River via the Siang could see a major increase in the population of 500 Ma zircons, with the small 500 Ma population observed in the samples older than the proposed rerouting delivered from transverse rivers draining north from the Indian plate to the Yarlung, or from Lhasa Block substrate. However, 42 percent of the Lohit River's zircon population is in the range 1.9 to 3.0 Ga, whereas this age range is absent from the Remi samples. This population is most likely derived from the Lesser Himalaya,

which began to exhume by 10 to 12 Ma (for example, Anczkiewicz and others, 2014), and therefore would be expected to contribute to the Lohit catchment by the time of the provenance change we observe in the Remi section.

Changes associated with eastward delivery of material from the Indo-Burman Ranges (IBR) accretionary prism.—As mentioned above, eastern tributaries drain the IBR, which consists of Paleogene turbidites derived from the eastern continuation of the arc in the east and Neogene Himalayan-derived off-scraped Bengal Fan deposits in the west. Sediments of rivers draining the IBR therefore contain a considerable proportion of arc-aged zircons as well as older grains (for example, the Dhansiri River; Bracciali and others, 2015). Westward propagation of the thrust belt progressively expanded the Neogene proportion of the drainage basin, thus potentially reducing the proportion of input from the Paleogene rocks with their arc-derived component. This scenario does not require the Remi section to be deposited by the trunk palaeo-Brahmaputra, since arc-aged grains would be derived from the east. Whilst this scenario could have resulted in the provenance changes we seek to explain the Remi section, it is less well suited to explaining the similar trend in the Siji section, as the rocks of the latter were clearly deposited by the trunk palaeo-Brahmaputra in view of the thermochronological data that indicate syntaxial derivation (Lang and others, 2016). Therefore, any change from eastern tributaries would need to feed into the trunk river. It seems unlikely that these tributaries could have such a substantial effect in terms of proportion input compared to the major trunk river. Furthermore, as discussed above, we argue on the basis of the zircon age characteristics that the Paleogene-Mesozoic grain-age spectra more closely resemble that of the arc west of, rather than east of the syntaxis.

In view of the above discussion, we prefer our initial interpretation for the dilution of arc-derived grains, that is, that it is caused by surface exposure of the Himalayan core of the rapidly exhuming Namche Barwa massif. Our data suggest that this happened >4 Ma, and the onset of rapid exhumation should therefore also precede this time, in keeping with the onset of rapid exhumation at 5 to 7 Ma inferred by Lang and others (2016). The general lack of young (<10 Ma) crystallization and cooling ages within our section is at variance with our interpretation of detritus derived from the rapidly exhuming Namche Barwa from >4 Ma discussed above. With regard to zircons, this discrepancy may be explained by the overall rarity of these young grains (for example, see fig. 5 of Bracciali and others, 2016). Furthermore, whilst the young (<10 Ma) zircon rims we record from 6 Ma in the Remi section might be considered supportive of syntaxial provenance (Bracciali and others, 2015), more recent work has shown that such aged grains are not unique to the syntaxis as previously believed; they have now also been recorded in the MCT zone outside the syntaxial region (Braden and others, 2018). With regard to the apatite U-Pb data, the paucity of U-Pb ages <6 to 5 Ma is likely related to large uncertainties on their U-Pb ages as a result of the typically high common Pb content, leading to rejection of young ages in the data screening process. We also note that apatite U-Pb/FT double dating may not be the optimal technique where very young U-Pb age populations are anticipated, due to the trade-off between the large spots (~30 μm diameter) typically desirable for U-Pb analysis by magnetic sector LA-ICPMS, and the smaller spots (~15 μm) typically preferred for AFT analysis in order to target defect-free zones of homogenous U concentration.

Drainage Development

The Yarlung-Siang-Brahmaputra connection.—The presence of Cretaceous-Early Paleogene zircons and apatites in the Sibo, Remi, and Siang successions since *ca.* 11 Ma indicates that the Yarlung-Brahmaputra connection was established by this time. This conclusion is compatible with previous provenance studies in the eastern Himalayan Sub-Himalaya (Cina and others, 2009; Chirouze and others, 2013; Lang and Huntington, 2014; Govin and others, 2018), which provided evidence for a

Yarlung-Brahmaputra connection established at least since deposition of the Middle Siwalik rocks, that is since Late Miocene times. Our data are also consistent with the presence of Transhimalayan detritus in the more distal records of the Surma Basin, Bangladesh and Bengal Fan since at least 18 Ma (Bracciali and others, 2015; Blum and others, 2018).

Some previous workers have proposed that the Yarlung-Brahmaputra routed via the Lohit prior to headward incision and capture by the Siang (for example, Robinson and others, 2014). Since the Siji succession contains material derived from the rapidly exhuming Namche Barwa massif from *ca.* 5.5 Ma, the Yarlung-Brahmaputra connection via the Siang must have existed since at least the Late Miocene (fig. 9). Our interpretation of the provenance change in the Remi section, in which the decrease in arc-aged material in units deposited after *ca.* 4 Ma is attributed to exposure and erosion of the Himalayan core of the Namche Barwa (see above) is consistent with this finding.

The Parlung-Siang connection.—Our U-Pb data show minor input of Early Cretaceous (and Late Jurassic; 100–150 Ma) zircon and apatite throughout the Sibo, Remi, and Siang successions. By contrast, the modern Siang River sediments show a major contribution of such zircon grains (Lang and others, 2013) (fig. 6). Early Cretaceous zircon U-Pb ages have been reported as a major age population of the Bomi-Chayu batholiths and may also be present in the Lohit Plutonic Suite (Cina and others, 2009; Haproff and others, 2013) (fig. 6). In the Transhimalayan region, this population contributed considerable detritus as far south as the forearc during the Paleogene (Orme and others, 2015). However, grains of this age do not form a major peak in the modern Yarlung; they are predominantly found only in tributaries that drain the far north of the Lhasa Block (Zhang and others, 2012; Carrapa and others, 2017). Presumably, this temporal change relates to topographic growth of the Trans-Himalaya, which then acted as a barrier to arrival of detritus from north of the suture zone.

Due to uncertainty of the paleo-location of our studied Siang, Remi, and Sibo sedimentary successions with respect to the trunk Brahmaputra River and its various tributaries draining these potential source regions, we can only speculate as to which region sourced the minor amount of Early-Cretaceous grains found in our samples. By contrast, the significant proportion of such grains in the modern Siang River implies a Bomi-Chayu source, in which such grains are prevalent. Therefore, the difference between the modern and paleo-samples suggests major river reorganization since deposition of the Sibo sediments, that is, more recent than *ca.* 800 ka.

The Bomi-Chayu granites are eroded by the Parlung River, which currently connects to the Siang via the narrow Parlung gorge north of Namche Barwa (figs. 1 and 9). Previous workers have proposed that the Parlung River originally flowed southeastward through a Yigong-Parlung-Lohit connection draining the Bomi-Chayu rocks (for example, Lang and Huntington, 2014) (fig. 9A). Initiation of the Parlung-Siang connection, implying reversal of the Parlung River, is inferred to have occurred during the Quaternary (Lang and Huntington, 2014) and probably during the past 1 Myr (King and others, 2016) (fig. 9C). We propose that the arrival of major amounts of Early Cretaceous aged zircons in the foreland basin within the last 190 to 770 kyr is a direct consequence of Parlung-Yigong capture by the Siang River. This Late Quaternary age is consistent with previous studies (Lang and Huntington, 2014; King and others, 2016) and implies that the Parlung capture could have been strongly influenced by glacial activity such as drainage-divide retreat or temporary ice damming (for example, Oskin and Burbank, 2005; Korup and others, 2010). The extremely high recent exhumation rates in the Parlung river area reported by King and others (2016) may originate from this capture and thus do not necessarily require northward growth of the Namche Barwa antiform.

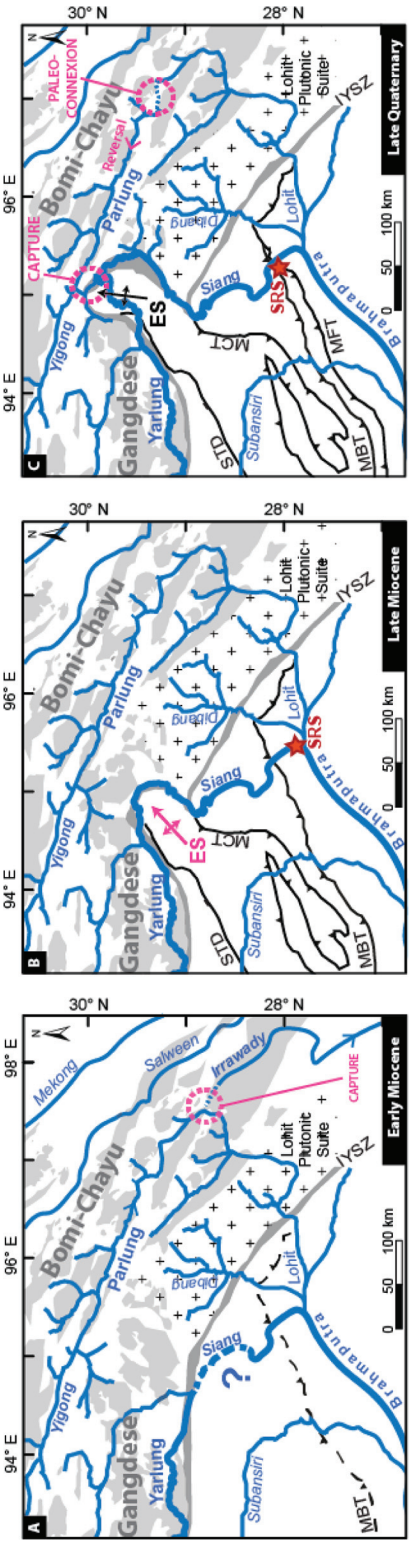

Fig. 9. Early-Miocene to Late Quaternary evolutionary model of the drainage system in the eastern syntaxis area (modified from Lang and Huntington, 2014) constructed using provenance analysis from this study, Lang and Huntington (2014), Clark and others (2004), Robinson and others (2014), and references therein. The question mark and the dotted drainage line indicates a potential paleo-drainage scenario in which the Yarlung-Brahmaputra connection existed through the Siang River since the Early Miocene, but other scenarios are possible such as a Yarlung-Brahmaputra connection through the Lohit River. Red star labeled SRS represents the location of the Sibo, Remi, and Siang sections. The arrows symbolize the northward growth of the antiformal Namche Barwa syntaxis. Abbreviations are: ES - Eastern Syntaxis, MFT - Main Frontal Thrust, MCT - Main Central Thrust, MBT - Main Boundary Thrust, STD - South Tibetan Detachment and IYSZ - Indus-Yarlung Suture Zone.

CONCLUSIONS

We have constrained the depositional ages of, and applied geochronological provenance techniques to, previously unstudied Himalayan foreland-basin Siwalik successions located in the extreme east of the orogen. The sections cover Middle to Upper Siwalik rocks deposited from Late-Miocene to Pleistocene times. The depositional dating combined with our detrital zircon U-Pb, and double-dated apatite U-Pb and AFT data, result in the following observations and consequent interpretations regarding the regional evolution:

(1) The previously developed hypothesis that the Yarlung-Brahmaputra fluvial connection has existed since at least the Late Miocene (for example, Lang and Huntington, 2014) is confirmed. We have demonstrated the systematic presence of Transhimalayan detritus throughout the Sibo, Remi and Siang successions, that is since at least Middle Siwalik times.

(2) The Transhimalayan zircon population decreases up section as the *ca.* 500 Ma population increases, with the most drastic change occurring sometime between 3.6 to 6.6 Ma. We interpret this trend to reflect progressive exhumation of the Namche Barwa syntaxis.

(3) Parlung-Yigong capture by the Siang River is constrained to have occurred after *ca.* 800 ka, as shown by the arrival of significant amounts of Early Cretaceous zircons characteristic of the Bomi-Chayu batholiths within this time interval. We suggest that this capture has enhanced erosion and exhumation rates in the region NE of the Namche Barwa syntaxis.

SUPPLEMENTARY MATERIAL

http://earth.geology.yale.edu/%7eajs/SupplementaryData/2018/Govin

1) Methodology
   – Luminescence Dating
   – Detrital Apatite Fission-Track and U-Pb Double Dating
   – Magnetostratigraphy
   – Detrital Zircon U-Pb Dating
2) Sample locations
3) Magnetostratigraphic data
4) Single-grain apatite fission-track - U-Pb data (4a), and plot showing relationship between U content and AFT ages (4b)
5) Zircon core and rim U-Pb data (5a); Zircon standard U-Pb data (5b).

ACKNOWLEDGMENTS

We acknowledge financial support from Marie Curie Initial Training Network iTECC funded by the EU REA under the FP7 implementation of the Marie Curie Action, under grant agreement 316966. We thank L. Gemignani for assistance in sample collection, M. Bernet, M. Balvay, F. Coeur and F. Senebier for helping in AFT mount preparation, R. Abrahami for sharing her experience in IRSL dating and S. Lowick for the IRSL dating. Isotope analysis at NIGL was funded by an award (IP-1500-1114) from NERC Services and Facilities Steering Committee. G. D-N acknowledges funding from the Marie Curie Career Integration Grant FP7 CIG grant 294282 'HIRESDAT' and Horizon 2020 ERC grant 649081 'MAGIC'. ISTerre is part of Labex OSUG@2020 (ANR10 LABX56). CM acknowledges support from Science Foundation Ireland (SFI) Grant Number 13/RC/2092, co-funded under the European Regional Development Fund. This paper benefitted from careful reviews by Peter DeCelles, Joel Saylor and the Associate Editor of AJS. First author Govin died after this paper was submitted; corrections were undertaken by co-authors.

REFERENCES CITED

Abrahami, R., Huyghe, P., van der Beek, P., Lowick, S., Carcaillet, J., and Chakraborty, T., 2018, Late Pleistocene - Holocene development of the Tista megafan (West Bengal, India): ^{10}Be cosmogenic and IRSL age constraints: Quaternary Science Reviews, v. 185, p. 69–90, https://doi.org/10.1016/j.quascirev.2018.02.001

Allen, R., Najman, Y. M. R., Carter, A., Barfod, D., Bickle, M. J., Chapman, H. J., Garzanti, E., Vezzoli, G., Andò, S., and Parrish, R. R., 2008, Provenance of the Tertiary sedimentary rocks of the Indo-Burman Ranges, Burma (Myanmar): Burman arc or Himalayan-derived?: Journal of the Geological Society, v. 165, p. 1045–1057, https://doi.org/10.1144/0016-76492007-143

Anczkiewicz, R., Chakraborty, S., Dasgupta, S., Mukhopadhyay, D., and Kołtonik, K., 2014, Timing, duration and inversion of prograde Barrovian metamorphism constrained by high resolution Lu-Hf garnet dating: A case study from the Sikkim Himalaya, NE India: Earth and Planetary Science Letters, v. 407, p. 70–81, https://doi.org/10.1016/j.epsl.2014.09.035

Bernet, M., van der Beek, P., Pik, R., Huyghe, P., Mugnier, J. L., Labrin, E., and Szulc, A., 2006, Miocene to Recent exhumation of the central Himalaya determined from combined detrital zircon fission–track and U/Pb analysis of Siwalik sediments, western Nepal: Basin Research, v. 18, n. 4, p. 393–412, https://doi.org/10.1111/j.1365-2117.2006.00303.x

Blum, M., Rogers, K., Gleason, J., Najman, Y., Cruz, J., and Fox, L., 2018, Allogenic and autogenic signals in the stratigraphic record of the deep-sea Bengal Fan: Scientific Reports, v. 8, p. 7–13, https://doi.org/10.1038/s41598-018-25819-5

Booth, A. L., Zeitler, P. K., Kidd, W. S., Wooden, J., Liu, Y., Idleman, B., Hren, M., and Chamberlain, C. P., 2004, U-Pb zircon constraints on the tectonic evolution of southeastern Tibet, Namche Barwa Area: American Journal of Science, v. 304, n. 10, p. 889–929, https://doi.org/10.2475/ajs.304.10.889

Booth, A. L., Chamberlain, C. P., Kidd, W. S., and Zeitler, P. K., 2009, Constraints on the metamorphic evolution of the eastern Himalayan syntaxis from geochronologic and petrologic studies of Namche Barwa: Geological Society of America Bulletin, v. 121, no. 3–4, p. 385–407, https://doi.org/10.1130/B26041.1

Bracciali, L., Najman, Y., Parrish, R. R., Akhter, S. H., and Millar, I., 2015, The Brahmaputra tale of tectonics and erosion: Early Miocene river capture in the Eastern Himalaya: Earth and Planetary Science Letters, v. 415, p. 25–37, https://doi.org/10.1016/j.epsl.2015.01.022

Bracciali, L., Parrish, R. R., Najman, Y., Smye, A., Carter, A., and Wijbrans, J. R., 2016, Plio-Pleistocene exhumation of the eastern Himalayan syntaxis and its domal pop-up: Earth Science Reviews, v. 160, p. 350–385, https://doi.org/10.1016/j.earscirev.2016.07.010

Braden, Z., Godin, L., and Cottle, J. M., 2017, Segmentation and rejuvenation of the Greater Himalayan sequence in western Nepal revealed by *in situ* U-Th/Pb monazite petrochronology: Lithos, v. 284–285, p. 751–765, https://doi.org/10.1016/j.lithos.2017.04.023

Braden, Z., Godin, L., Cottle, J., and Yakymchuk, C., 2018, Renewed late Miocene (<8 Ma) hinterland ductile thrusting, western Nepal Himalaya: Geology, v. 46, n. 6, p. 503–506, https://doi.org/10.1130/G40097.1

Brookfield, M., 1998, The evolution of the great river systems of southern Asia during the Cenozoic India-Asia collision: Rivers draining southwards: Geomorphology, v. 22, n. 3–4, p. 285–312, https://doi.org/10.1016/S0169-555X(97)00082-2

Burbank, D. W., Beck, R. A., and Mulder, T., 1996, The Himalayan foreland basin, *in* Yin, A., and Harrison, M. T., editors, The Tectonic Evolution of Asia: Cambridge, Cambridge University Press, p. 149–188.

Burg, J.-P., Davy, P., Nievergelt, P., Oberli, F., Seward, D., Diao, Z., and Meier, M., 1997, Exhumation during crustal folding in the Namche–Barwa syntaxis: Terra Nova, v. 9, n. 2, p. 53–56, https://doi.org/10.1111/j.1365-3121.1997.tb00001.x

Burg, J.-P., Nievergelt, P., Oberli, F., Seward, D., Davy, P., Maurin, J.-C., Diao, Z., and Meier, M., 1998, The Namche Barwa syntaxis: Evidence for exhumation related to compressional crustal folding: Journal of Asian Earth Sciences, v. 16, n. 2–3, p. 239–252, https://doi.org/10.1016/S0743-9547(98)00002-6

Butler, R., 1992, Paleomagnetism: Magnetic domains to geologic terrains: Oxford, England, Backwell Scientific Publication, 319 p.

Carlson, W. D., Donelick, R. A., and Ketcham, R. A., 1999, Variability of apatite fission-track annealing kinetics: I. Experimental results: American Mineralogist, v. 84, n. 9, p. 1213–1223, https://doi.org/10.2138/am-1999-0901

Carrapa, B., Faiz bin Hassim, M., Kapp, P. A., DeCelles, P. G., and Gehrels, G., 2017, Tectonic and erosional history of southern Tibet recorded by detrital chronological signatures along the Yarlung River drainage: Geological Society of America Bulletin, v. 129, n. 5-6, p. 570–581, https://doi.org/10.1130/B31587.1

Catlos, E. J., Dubey, C. S., Harrison, T. M., and Edwards, M. A., 2004, Late Miocene movement within the Himalayan Main Central Thrust shear zone, Sikkim, north-east India: Journal of Metamorphic Geology, v. 22, n. 3, p. 207–226, https://doi.org/10.1111/j.1525-1314.2004.00509.x

Cherniak, D. J., and Watson, E. B., 2000, Pb diffusion in zircon: Chemical Geology, v. 172, n. 1–2, p. 5–24, https://doi.org/10.1016/S0009-2541(00)00233-3

Chew, D. M., Sylvester, P. J., and Tubrett, M. N., 2011, U–Pb and Th–Pb dating of apatite by LA-ICPMS: Chemical Geology, v. 280, n. 1–2, p. 200–216, https://doi.org/10.1016/j.chemgeo.2010.11.010

Chirouze, F., Dupont-Nivet, G., Huyghe, P., van der Beek, P., Chakraborti, T., Bernet, M., and Erens, V., 2012, Magnetostratigraphy of the Neogene Siwalik Group in the far eastern Himalaya: Kameng section, Arunachal Pradesh, India: Journal of Asian Earth Sciences, v. 44, p. 117–135, https://doi.org/10.1016/j.jseaes.2011.05.016

Chirouze, F., Huyghe, P., van der Beek, P., Chauvel, C., Chakraborty, T., Dupont-Nivet, G., and Bernet, M., 2013, Tectonics, exhumation, and drainage evolution of the eastern Himalaya since 13 Ma from detrital

geochemistry and thermochronology, Kameng River Section, Arunachal Pradesh: Geological Society of America Bulletin, v. 125, n. 3–4, p. 523–538, https://doi.org/10.1130/B30697.1
Chirouze, F., Huyghe, P., Chauvel, C., van der Beek, P., Bernet, M., and Mugnier, J.-L., 2015, Stable drainage pattern and variable exhumation in the western Himalaya since the middle Miocene: The Journal of Geology, v. 123, n. 1, p. 1–20, https://doi.org/10.1086/679305
Chiu, H.-Y., Chung, S.-L., Wu, F.-Y., Liu, D., Liang, Y.-H., Lin, I.-J., Iizuka, Y., Xie, L.-W., Wang, Y., and Chu, M.-F., 2009, Zircon U–Pb and Hf isotopic constraints from eastern Transhimalayan batholiths on the precollisional magmatic and tectonic evolution in southern Tibet: Tectonophysics, v. 477, n. 1–2, p. 3–19, https://doi.org/10.1016/j.tecto.2009.02.034
Chu, M.-F., Chung, S.-L., Song, B., Liu, D., O'Reilly, S. Y., Pearson, N. J., Ji, J., and Wen, D.-J., 2006, Zircon U-Pb and Hf isotope constraints on the Mesozoic tectonics and crustal evolution of southern Tibet: Geology, v. 34, n. 9, p. 745–748, https://doi.org/10.1130/G22725.1
Cina, S. E., Yin, A., Grove, M., Dubey, C. S., Shukla, D. P., Lovera, O. M., Kelty, T. K., Gehrels, G. E., and Foster, D. A., 2009, Gangdese arc detritus within the eastern Himalayan Neogene foreland basin: Implications for the Neogene evolution of the Yalu–Brahmaputra River system: Earth and Planetary Science Letters, v. 285, n. 1–2, p. 150–162, https://doi.org/10.1016/j.epsl.2009.06.005
Clark, M. K., Schoenbohm, L. M., Royden, L. H., Whipple, K. X., Burchfiel, B. C., Zhang, X., Tang, W., Wang, E., and Chen, L., 2004, Surface uplift, tectonics, and erosion of eastern Tibet from large–scale drainage patterns: Tectonics, v. 23, n. 1, TC1006, https://doi.org/10.1029/2002TC001402
Clift, P. D., Blusztajn, J., and Nguyen, A. D., 2006, Large–scale drainage capture and surface uplift in eastern Tibet–SW China before 24 Ma inferred from sediments of the Hanoi Basin, Vietnam: Geophysical Research Letters, v. 33, n. 19, L19403, https://doi.org/10.1029/2006GL027772
Cochrane, R., Spikings, R. A., Chew, D., Wotzlaw, J.-F., Chiaradia, M., Tyrrell, S., Schaltegger, U., and Van der Lelij, R., 2014, High temperature (> 350 °C) thermochronology and mechanisms of Pb loss in apatite: Geochimica et Cosmochimica Acta, v. 127, p. 39–56, https://doi.org/10.1016/j.gca.2013.11.028
Coutand, I., Barrier, L., Govin, G., Grujic, D., Hoorn, C., Dupont–Nivet, G., and Najman, Y., 2016, Late Miocene–Pleistocene evolution of India–Eurasia convergence partitioning between the Bhutan Himalaya and the Shillong plateau: New evidences from foreland basin deposits along the Dungsam Chu section, Eastern Bhutan: Tectonics, v. 35, n. 12, p. 2963–2994, https://doi.org/10.1002/2016TC004258
Curray, J. R., Moore, D. G., Lawver, L. A., Emmel, F. J., Raitt, R. W., Henry, M., and Kieckhefer, R., 1979, Tectonics of the Andaman Sea and Burma: Convergent margins, *in* Watkins, J. S., Montadert, L., and Dickerson, P. W., editors, Geological and geophysical investigations of continental margins: American Association of Petroleum Geologists Memoir 29, p. 189–198, https://doi.org/10.1306/M29405C12
DeCelles, P. G., Gehrels, G. E., Quade, J., Ojha, T. P., Kapp, P. A., and Upreti, B. N., 1998, Neogene foreland basin deposits, erosional unroofing, and the kinematic history of the Himalayan fold-thrust belt, western Nepal: Geological Society of America Bulletin, v. 110, n. 1, p. 2–21, https://doi.org/10.1130/0016-7606(1998)110<0002:NFBDEU>2.3.CO;2
DeCelles, P. G., Gehrels, G. E., Najman, Y., Martin, A., Carter, A., and Garzanti, E., 2004, Detrital geochronology and geochemistry of Cretaceous–Early Miocene strata of Nepal: Implications for timing and diachroneity of initial Himalayan orogenesis: Earth and Planetary Science Letters, v. 227, n. 3–4, p. 313–330, https://doi.org/10.1016/j.epsl.2004.08.019
DeCelles, P. G., Kapp, P., Gehrels, G. E., and Ding, L., 2014, Paleocene-Eocene foreland basin evolution in the Himalaya of southern Tibet and Nepal: Implications for the age of initial India-Asia collision: Tectonics, v. 33, n. 5, p. 824–849, https://doi.org/10.1002/2014TC003522
DeCelles, P. G., Carrapa, B., Gehrels, G. E., Chakraborty, T., and Ghosh, P., 2016, Along-strike continuity of structure, stratigraphy, and kinematic history in the Himalayan thrust belt: The view from Northeastern India: Tectonics, v. 35, n. 12, p. 2995–3027, https://doi.org/10.1002/2016TC004298
Ding, L., Zhong, D., Yin, A., Kapp, P., and Harrison, T. M., 2001, Cenozoic structural and metamorphic evolution of the eastern Himalayan syntaxis (Namche Barwa): Earth and Planetary Science Letters, v. 192, n. 3, p. 423–438, https://doi.org/10.1016/S0012-821X(01)00463-0
Donelick, R. A., O'Sullivan, P. B., and Ketcham, R. A., 2005, Apatite fission-track analysis: Reviews in Mineralogy and Geochemistry, v. 58, p. 49–94, https://doi.org/10.2138/rmg.2005.58.3
Finnegan, N. J., Hallet, B., Montgomery, D. R., Zeitler, P. K., Stone, J. O., Anders, A. M., and Yuping, L., 2008, Coupling of rock uplift and river incision in the Namche Barwa–Gyala Peri massif, Tibet: Geological Society of America Bulletin, v. 120, n. 1–2, p. 142–155, https://doi.org/10.1130/B26224.1
Galbraith, R. F., 2005, Statistics for fission track analysis: Boca Raton, Florida, CRC Press, 218 p., https://doi.org/10.1201/9781420034929
Gansser, A., 1983, Geology of the Bhutan Himalaya: Mémoires de al Société Helvétique des Sciences Naturelles, v. 96, p. 181.
Gautam, P., and Fujiwara, Y., 2000, Magnetic polarity stratigraphy of Siwalik Group sediments of Karnali River section in western Nepal: Geophysical Journal International, v. 142, n. 3, p. 812–824, https://doi.org/10.1046/j.1365-246x.2000.00185.x
Gehrels, G. E., Valencia, V. A., and Ruiz, J., 2008, Enhanced precision, accuracy, efficiency, and spatial resolution of U–Pb ages by laser ablation–multicollector–inductively coupled plasma–mass spectrometry: Geochemistry, Geophysics, Geosystems, v. 9, n. 3, https://doi.org/10.1029/2007GC001805
Gehrels, G., Kapp, P., DeCelles, P., Pullen, A., Blakey, R., Weislogel, A., Ding, L., Guynn, J., Martin, A., McQuarrie, N., and Yin, A., 2011, Detrital zircon geochronology of pre–Tertiary strata in the Tibetan–Himalayan orogen: Tectonics, v. 30, n. 5, TC5016, https://doi.org/10.1029/2011TC002868
Godin, L., Grujic, D., Law, R. D., and Searle, M. P., 2006, Channel flow, ductile extrusion, and exhumation in continental collision zones: An introduction, *in* Law, R. D., Searle, M. P., and Godin, L., editors, Channel Flow, Ductive Extrusion and Exhumation in Continental Collision Zones: Geological Society, London, Special Publications, v. 268, p. 1–23, https://doi.org/10.1144/GSL.SP.2006.268.01.01

Govin, G., ms, 2017, Tectonic-Erosion Interactions: Insights from the palaeo-drainage of the Brahmaputra River: Lancaster, United Kingdom, Lancaster University, 331 p., Ph. D. thesis, doi:10.17635/lancaster/thesis/116

Govin, G., Najman, Y. M. R., Copley, A., Millar, I., van der Beek, P., Huyghe, P., Grujic, D., and Davenport, J., 2018, Timing and mechanism of the rise of the Shillong Plateau in the Himalayan foreland: Geology, v. 46, n. 3, p. 279–282, https://doi.org/10.1130/G39864.1

Gradstein, F. M., Ogg, J. G., Schmitz, M., and Ogg, G., 2012, The geologic time scale 2012: The Netherlands, Elsevier, 1176 p., https://doi.org/10.1016/C2011-1-08249-8

Haproff, P., Yin, A., and Dubey, C., 2013, Tectonic framework of the easternmost Himalayan orogen based on U-Pb zircon geochronology and detailed geologic mapping, NE India: AGU Fall Meeting Abstracts 2013, p. 2422.

Haproff, P. J., Zuza, A. V., and Yin, A., 2018, West-directed thrusting south of the eastern Himalayan syntaxis indicates clockwise crustal flow at the indenter corner during the India-Asia collision: Tectonophysics, v. 722, p. 277–285, https://doi.org/10.1016/j.tecto.2017.11.001

Harrison, T. M., Copeland, P., Hall, S. A., Quade, J., Burner, S., Ojha, T. P., and Kidd, W. S., 1993, Isotopic preservation of Himalayan/Tibetan uplift, denudation, and climatic histories of two molasse deposits: The Journal of Geology, v. 101, n. 2, p. 157–175, https://doi.org/10.1086/648214

Hébert, R., Bezard, R., Guilmette, C., Dostal, J., Wang, C. S., and Liu, Z. F., 2012, The Indus–Yarlung Zangbo ophiolites from Nanga Parbat to Namche Barwa syntaxes, southern Tibet: First synthesis of petrology, geochemistry, and geochronology with incidences on geodynamic reconstructions of Neo-Tethys: Gondwana Research, v. 22, n. 2, p. 377–397, https://doi.org/10.1016/j.gr.2011.10.013

Hodges, K. V., 2000, Tectonics of the Himalaya and southern Tibet from two perspectives: Geological Society of America Bulletin, v. 112, n. 3, p. 324–350, https://doi.org/10.1130/0016-7606(2000)112<324:TOTHAS>2.0.CO;2

Hoskin, P. W. O., and Schaltegger, U., 2003, The composition of zircon and igneous and metamorphic petrogenesis, *in* Hanchar, J. M., and Hoskin, P. W. O. editors, Zircon: Reviews in Mineralogy and Geochemistry, v. 53, p. 27–62, https://doi.org/10.2113/0530027

Hu, X., Garzanti, E., Moore, T., and Raffi, I., 2015, Direct stratigraphic dating of India-Asia collision onset at the Selandian (middle Paleocene, 59 ± 1 Ma): Geology, v. 43, n. 10, p. 859–862, https://doi.org/10.1130/G36872.1

Huang, C. M., Zhao, Z. D., Li, G. M., Zhu, D. C., Liu, D., and Shi, Q. S., 2017, Leucogranites in Lhozag, southern Tibet: Implications for the tectonic evolution of the eastern Himalaya: Lithos, v. 294–295, p. 246–262, https://doi.org/10.1016/j.lithos.2017.09.014

Huyghe, P., Mugnier, J. L., Gajurel, A. P., and Delcaillau, B., 2005, Tectonic and climatic control of the changes in the sedimentary record of the Karnali River section (Siwaliks of western Nepal): Island Arc, v. 14, n. 4, p. 311–327, https://doi.org/10.1111/j.1440-1738.2005.00500.x

Ji, W-Q., Wu, F-Y., Chung, S-L., Li, J-X., and Liu, C-Z., 2009, Zircon U-Pb geochronology and Hf isotopic constraints on petrogenesis of the Gangdese batholith, southern Tibet: Chemical Geology, v. 262, n. 3–4, p. 229–245, https://doi.org/10.1016/j.chemgeo.2009.01.020

Johnson, N. M., Stix, J., Tauxe, L., Cerveny, P. F., and Tahirkheli, R. A. K., 1985, Paleomagnetic chronology, fluvial processes, and tectonic implications of the Siwalik deposits near Chinji Village, Pakistan: The Journal of Geology, v. 93, n. 1, p. 27–40, https://doi.org/10.1086/628917

Kellett, D. A., Grujic, D., Coutand, I., Cottle, J., and Mukul, M., 2013, The South Tibetan detachment system facilitates ultra rapid cooling of granulite–facies rocks in Sikkim Himalaya: Tectonics, v. 32, n. 2, p. 252–270, https://doi.org/10.1002/tect.20014

King, G. E., Herman, F., and Guralnik, B., 2016, Northward migration of the eastern Himalayan syntaxis revealed by OSL thermochronometry: Science, v. 353, n. 6301, p. 800–804, https://doi.org/10.1126/science.aaf2637

Korup, O., Montgomery, D. R., and Hewitt, K., 2010, Glacier and landslide feedbacks to topographic relief in the Himalayan syntaxes: Proceedings of the National Academy of Sciences of the United States of America, v. 107, n. 12, p. 5317–5322, https://doi.org/10.1073/pnas.0907531107

Koymans, M. R., Langereis, C. G., Pastor-Galán, D., and van Hinsbergen, D. J., 2016, Paleomagnetism.org: An online multi-platform open source environment for paleomagnetic data analysis: Computers & Geosciences, v. 93, p. 127–137, https://doi.org/10.1016/j.cageo.2016.05.007

Lang, K. A., and Huntington, K. W., 2014, Antecedence of the Yarlung–Siang–Brahmaputra River, eastern Himalaya: Earth and Planetary Science Letters, v. 397, p. 145–158, https://doi.org/10.1016/j.epsl.2014.04.026

Lang, K. A., Huntington, K. W., and Montgomery, D. R., 2013, Erosion of the Tsangpo Gorge by megafloods, Eastern Himalaya: Geology, v. 41, n. 9, p. 1003–1006, https://doi.org/10.1130/G34693.1

Lang, K. A., Huntington, K. W., Burmester, R., and Housen, B., 2016, Rapid exhumation of the eastern Himalayan syntaxis since the late Miocene: Geological Society of America Bulletin, v. 128, n. 9–10, p. 1403–1422, https://doi.org/10.1130/B31419.1

Larsen, I. J., and Montgomery, D. R., 2012, Landslide erosion coupled to tectonics and river incision: Nature Geoscience, v. 5, p. 468–473, https://doi.org/10.1038/ngeo1479

Le Fort, P., 1975, Himalayas: The collided range present knowledge of the continental arc: American Journal of Science, v. 275-A, p. 1–44.

Leary, R. J., DeCelles, P. G., Quade, J., Gehrels, G. E., and Waanders, G., 2016, The Liuqu Conglomerate, southern Tibet: Early Miocene basin development related to deformation within the Great Counter Thrust system: Lithosphere, v. 8, n. 5, p. 427–450, https://doi.org/10.1130/L542.1

Liang, Y.-H., Chung, S.-L., Liu, D., Xu, Y., Wu, F.-Y., Yang, J.-H., Wang, Y., and Lo, C.-H., 2008, Detrital zircon evidence from Burma for reorganization of the eastern Himalayan river system: American Journal of Science, v. 308, n. 4, p. 618–638, https://doi.org/10.2475/04.2008.08

Licht, A., France-Lanord, C., Reisberg, L., Fontaine, C., Soe, A. N., and Jaeger, J.-J., 2013, A palaeo Tibet–Myanmar connection? Reconstructing the Late Eocene drainage system of central Myanmar using a multi-proxy approach: Journal of the Geological Society, v. 170, n. 6, p. 929–939, https://doi.org/10.1144/jgs2012-126

Licht, A., Reisberg, L., France-Lanord, C., Naing Soe, A., and Jaeger, J.-J., 2016, Cenozoic evolution of the central Myanmar drainage system: Insights from sediment provenance in the Minbu Sub-Basin: Basin Research, v. 28, n. 2, p. 237–251, https://doi.org/10.1111/bre.12108

Liu, X. C., Wu, F. Y., Yu, L. J., Liu, Z. C., Ji, W. Q., and Wang, J. G., 2016, Emplacement age of leucogranite in the Kampa Dome, southern Tibet: Tectonophysics, v. 667, p. 163–175, https://doi.org/10.1016/j.tecto.2015.12.001

Long, S. P., McQuarrie, N., Tobgay, T., Coutand, I., Cooper, F. J., Reiners, P. W., Wartho, J.-A., and Hodges, K. V., 2012, Variable shortening rates in the eastern Himalayan thrust belt, Bhutan: Insights from multiple thermochronologic and geochronologic data sets tied to kinematic reconstructions: Tectonics, v. 31, n. 5, TC5004, https://doi.org/10.1029/2012TC003155

Ludwig, K. R., 2003, User's manual for Isoplot 3.00: A geochronological toolkit for Microsoft Excel, v. 4: Berkeley, California, Berkeley Geochronological Center.

Luirei, K., and Bhakuni, S., 2008, Ground tilting in Likhabali area along the frontal part of Arunachal Himalaya: Evidence of neotectonics: Journal of the Geological Society of India, v. 71, n. 6, p. 780–786.

Mark, C., Cogné, N., and Chew, D., 2016, Tracking exhumation and drainage divide migration of the Western Alps: A test of the apatite U-Pb thermochronometer as a detrital provenance tool: Geological Society of America Bulletin, v. 128, n. 9–10, p. 1439–1460, https://doi.org/10.1130/B31351.1

Maurin, T., and Rangin, C., 2009, Structure and kinematics of the Indo-Burmese Wedge: Recent and fast growth of the outer wedge: Tectonics, v. 28, n. 2, TC2010, https://doi.org/10.1029/2008TC002276

McFadden, P. L., and McElhinny, M. W., 1988, The combined analysis of remagnetization circles and direct observations in palaeomagnetism: Earth and Planetary Science Letters, v. 87, n. 1, p. 161–172, https://doi.org/10.1016/0012-821X(88)90072-6

McQuarrie, N., Robinson, D., Long, S., Tobgay, T., Grujic, D., Gehrels, G., and Ducea, M., 2008, Preliminary stratigraphic and structural architecture of Bhutan: Implications for the along strike architecture of the Himalayan system: Earth and Planetary Science Letters, v. 272, n. 1–2, p. 105–117, https://doi.org/10.1016/j.epsl.2008.04.030

Meigs, A. J., Burbank, D. W., and Beck, R. A., 1995, Middle-late Miocene (> 10 Ma) formation of the Main Boundary thrust in the western Himalaya: Geology, v. 23, n. 5, p. 423–426, https://doi.org/10.1130/0091-7613(1995)023<0423:MLMMFO>2.3.CO;2

Mo, X., Hou, Z., Niu, Y., Dong, G., Qu, X., Zhao, Z., and Yang, Z., 2007, Mantle contributions to crustal thickening during continental collision: Evidence from Cenozoic igneous rocks in southern Tibet: Lithos, v. 96, n. 1–2, p. 225–242, https://doi.org/10.1016/j.lithos.2006.10.005

Najman, Y., Garzanti, E., Pringle, M., Bickle, M., Stix, J., and Khan, I., 2003, Early-Middle Miocene paleodrainage and tectonics in the Pakistan Himalaya: Geological Society of America Bulletin, v. 115, n. 10, p. 1265–1277, https://doi.org/10.1130/B25165.1

Najman, Y., Appel, E., Boudagher–Fadel, M., Bown, P., Carter, A., Garzanti, E., Godin, L., Han, J., Liebke, U., Oliver, G., Parrish, R., and Vezzoli, G., 2010, Timing of India–Asia collision: Geological, biostratigraphic, and palaeomagnetic constraints: Journal of Geophysical Research: Solid Earth, v. 115, B12416, https://doi.org/10.1029/2010JB007673

Najman, Y. M. R., Allen, R., Willett, E. A. F., Carter, A., Barfod, D., Garzanti, E., Wijbrans, J., Bickle, M. J., Vezzoli, G., Andò, S., Oliver, G., and Uddin, M. J., 2012, The record of Himalayan erosion preserved in the sedimentary rocks of the Hatia Trough of the Bengal Basin and the Chittagong Hill Tracts, Bangladesh: Basin Research, v. 24, n. 5, p. 499–519, https://doi.org/10.1111/j.1365-2117.2011.00540.x

Ojha, T. P., Butler, R. F., Quade, J., DeCelles, P. G., Richards, D., and Upreti, B. N., 2000, Magnetic polarity stratigraphy of the Neogene Siwalik Group at Khutia Khola, far western Nepal: Geological Society of America Bulletin, v. 112, n. 3, p. 424-434, https://doi.org/10.1130/0016-7606(2000)112<424:MPSOTN>2.0.CO;2

Ojha, T. P., Butler, R. F., DeCelles, P. G., and Quade, J., 2009, Magnetic polarity stratigraphy of the Neogene foreland basin deposits of Nepal: Basin Research, v. 21, n. 1, p. 61–90, https://doi.org/10.1111/j.1365-2117.2008.00374.x

Orme, D. A., Carrapa, B., and Kapp, P., 2015, Sedimentology, provenance and geochronology of the upper Cretaceous-lower Eocene western Xigaze forearc basin, southern Tibet: Basin Research, v. 27, n. 4, p. 387–411, https://doi.org/10.1111/bre.12080

Oskin, M., and Burbank, D. W., 2005, Alpine landscape evolution dominated by cirque retreat: Geology, v. 33, n. 12, p. 933–936, https://doi.org/10.1130/G21957.1

Quade, J., Cater, J. M. L., Ojha, T. P., Adam, J., and Harrison, T. M., 1995, Late Miocene environmental change in Nepal and the northern Indian subcontinent: Stable isotopic evidence from paleosols: Geological Society of America Bulletin, v. 107, n. 12, p. 1381–1397, https://doi.org/10.1130/0016-7606(1995)107<1381:LMECIN>2.3.CO;2

Robinson, R. A. J., Brezina, C. A., Parrish, R. R., Horstwood, M. S. A., Oo, N. W., Bird, M. I., Thein, M., Walters, A. S., Oliver, G. J. H., and Zaw, K., 2014, Large rivers and orogens: The evolution of the Yarlung Tsangpo–Irrawaddy system and the eastern Himalayan syntaxis: Gondwana Research, v. 26, n. 1, p. 112–121, https://doi.org/10.1016/j.gr.2013.07.002

Sanyal, P., Bhattacharya, S. K., Kumar, R., Ghosh, S. K., and Sangode, S. J., 2004, Mio–Pliocene monsoonal record from Himalayan foreland basin (Indian Siwalik) and its relation to vegetational change: Palaeogeography, Palaeoclimatology, Palaeoecology, v. 205, n. 1–2, p. 23–41, https://doi.org/10.1016/j.palaeo.2003.11.013

Schmitz, M. D., and Bowring, S. A., 2003, Constraints on the thermal evolution of continental lithosphere

from U-Pb accessory mineral thermochronometry of lower crustal xenoliths, southern Africa: Contributions to Mineralogy and Petrology, v. 144, n. 5, p. 592–618, https://doi.org/10.1007/s00410-002-0419-9
Seward, D., and Burg, J.-P., 2008, Growth of the Namche Barwa Syntaxis and associated evolution of the Tsangpo Gorge: Constraints from structural and thermochronological data: Tectonophysics, v. 451, n. 1, p. 282–289, https://doi.org/10.1016/j.tecto.2007.11.057
Srivastava, P., Bhakuni, S. S., Luirei, K., and Misra, D. K., 2009, Morpho–sedimentary records at the Brahmaputra River exit, NE Himalaya: Climate–tectonic interplay during the Late Pleistocene–Holocene: Journal of Quaternary Science, v. 24, n. 2, p. 175–188, https://doi.org/10.1002/jqs.1190
Stacey, J. S., and Kramers, J. D., 1975, Approximation of terrestrial lead isotope evolution by a two-stage model: Earth and Planetary Science Letters, v. 26, n. 2, p. 207–221, https://doi.org/10.1016/0012-821X(75)90088-6
Szulc, A. G., Najman, Y., Sinclair, H. D., Pringle, M., Bickle, M., Chapman, H., Garzanti, E., Ando, S., Huyghe, P., Mugnier, J. L., Ohja, T., and DeCelles, P., 2006, Tectonic evolution of the Himalaya constrained by detrital ^{40}Ar–^{39}Ar, Sm–Nd and petrographic data from the Siwalik foreland basin succession, SW Nepal: Basin Research, v. 18, n. 4, p. 375–391, https://doi.org/10.1111/j.1365-2117.2006.00307.x
Thiede, R. C., and Ehlers, T. A., 2013, Large spatial and temporal variations in Himalayan denudation: Earth and Planetary Science Letters, v. 371–372, p. 278–293, https://doi.org/10.1016/j.epsl.2013.03.004
Turab, S. A., Stüwe, K., Stuart, F. M., Chew, D. M., and Cogne, N., 2017, Tectonics drives rapid exhumation of the western Himalayan syntaxis: Evidence from low-temperature thermochronometry of the Neelum valley region, Pakistan: Lithosphere, 9, n. 6, p. 874–888, https://doi.org/10.1130/L626.1
van der Beek, P., Robert, X., Mugnier, J. L., Bernet, M., Huyghe, P., and Labrin, E., 2006, Late Miocene–recent exhumation of the central Himalaya and recycling in the foreland basin assessed by apatite fission–track thermochronology of Siwalik sediments, Nepal: Basin Research, v. 18, n. 4, p. 413–434, https://doi.org/10.1111/j.1365-2117.2006.00305.x
Verma, P. K., editor, 1999, Geological Studies in the Eastern Himalayas: Delhi, India, Pilgrim Books, 264 p.
Vermeesch, P., 2012, On the visualisation of detrital age distributions: Chemical Geology, v. 312–313, p. 190–194, https://doi.org/10.1016/j.chemgeo.2012.04.021
Vögeli, N., Huyghe, P., van der Beek, P., Najman, Y., Garzanti, E., and Chauvel, C., 2017b, Weathering regime in the Eastern Himalaya since the mid-Miocene: Indications from detrital geochemistry and clay mineralogy of the Kameng River Section, Arunachal Pradesh, India: Basin Research, v. 30, n. 1, p. 59–74, https://doi.org/10.1111/bre.12242
Vögeli, N., Najman, Y., van der Beek, P., Huyghe, P., Wynn, P. M., Govin, G., van der Veen, I., and Sachse, D., 2017a, Lateral variations in vegetation in the Himalaya since the Miocene and implications for climate evolution: Earth and Planetary Science Letters, v. 471, p. 1–9, https://doi.org/10.1016/j.epsl.2017.04.037
Wang, J. G., Wu, F.-Y., Tan, X.-C., and Liu, C.-Z., 2014, Magmatic evolution of the Western Myanmar Arc documented by U–Pb and Hf isotopes in detrital zircon: Tectonophysics, v. 612–613, p. 97–105, https://doi.org/10.1016/j.tecto.2013.11.039
Webb, A. A. G., Yin, A., and Dubey, C. S., 2013, U-Pb zircon geochronology of major lithologic units in the eastern Himalaya: Implications for the origin and assembly of Himalayan rocks: Geological Society of America Bulletin, v. 125, n. 3–4, p. 499–522, https://doi.org/10.1130/B30626.1
Xu, Y.-G., Yang, Q.-J., Lan, J.-B., Luo, Z.-Y., Huang, X.-L., Shi, Y.-R., and Xie, L.-W., 2012, Temporal–spatial distribution and tectonic implications of the batholiths in the Gaoligong–Tengliang–Yingjiang area, western Yunnan: Constraints from zircon U–Pb ages and Hf isotopes: Journal of Asian Earth Sciences, v. 53, p. 151–175, https://doi.org/10.1016/j.jseaes.2011.06.018
Yin, A., and Harrison, T. M., 2000, Geologic evolution of the Himalayan-Tibetan orogen: Annual Review of Earth and Planetary Sciences, v. 28, n. 1, p. 211–280, https://doi.org/10.1146/annurev.earth.28.1.211
Yin, A., Dubey, C. S., Kelty, T. K., Gehrels, G. E., Chou, C. Y., Grove, M., and Lovera, O., 2006, Structural evolution of the Arunachal Himalaya and implications for asymmetric development of the Himalayan orogen: Current Science, v. 90, n. 2, p. 195–200.
Yin, A., Dubey, C. S., Kelty, T. K., Webb, A. A. G., Harrison, T. M., Chou, C. Y., and Célérier, J., 2010, Geologic correlation of the Himalayan orogen and Indian craton: Part 2. Structural geology, geochronology, and tectonic evolution of the Eastern Himalaya: Geological Society of America Bulletin, v. 122, n. 3–4, p. 360–395, https://doi.org/10.1130/B26461.1
Zattin, M., Andreucci, B., Thomson, S. N., Reiners, P. W., and Talarico, F. M., 2012, New constraints on the provenance of the ANDRILL AND–2A succession (western Ross Sea, Antarctica) from apatite triple dating: Geochemistry, Geophysics, Geosystems, v. 13, n. 10, Q10016, https://doi.org/10.1029/2012GC004357
Zeitler, P. K., Meltzer, A. S., Koons, P. O., Craw, D., Hallet, B., Chamberlain, C. P., Kidd, W. S. F., Park, S. K., Seeber, L., Bishop, M., and Shroder, J., 2001, Erosion, Himalayan geodynamics, and the geomorphology of metamorphism: GSA Today, v. 11, n. 1, p. 4–9, https://doi.org/10.1130/1052-5173(2001)011<0004:EHGATG>2.0.CO;2
Zeitler, P. K., Meltzer, A. S., Brown, L., Kidd, W. S. F., Lim, C., and Enkelmann, E., 2014, Tectonics and topographic evolution of Namche Barwa and the easternmost Lhasa block, Tibet, *in* Nie, J., Hoke, G. D., and Horton, B. K., editor, Toward an Improved Understanding of Uplift Mechanisms and the Elevation History of the Tibetan Plateau: Geological Society of America Special Papers, v. 507, p. 23–58, https://doi.org/10.1130/2014.2507(02)
Zhang, J. Y., Yin, A., Liu, W. C., Wu, F. Y., Lin, D., and Grove, M., 2012, Coupled U-Pb dating and Hf isotopic analysis of detrital zircon of modern river sand from the Yalu River (Yarlung Tsangpo) drainage system in southern Tibet: Constraints on the transport processes and evolution of Himalayan rivers: Geological Society of America Bulletin, v. 124, n. 9–10, p. 1449–1473, https://doi.org/10.1130/B30592.1